

Adaptive Local Combining with Decentralized Decoding for Distributed Massive MIMO

Mohd Saif Ali Khan*, Karthik R.M.⁺ and Samar Agnihotri*

*School of Computing & EE, Indian Institute of Technology Mandi, HP, India

⁺Ericsson India Pvt. Ltd., Chennai, TN, India

Email: d21013@students.iitmandi.ac.in, karthik.r.m@ericsson.com, samar@iitmandi.ac.in

Abstract

Efficient uplink processing in distributed massive multiple-input multiple-output (D-mMIMO) systems requires both effective local combining and scalable decoding to significantly mitigate inter-user interference. Recent zero-forcing (ZF)-based combining schemes, such as partial full-pilot ZF (PFZF) and protected weak PFZF (PWPFZF), rely on heuristic threshold-based user grouping that may lead to inefficient utilization of spatial degrees of freedom across access points (APs). To address this limitation, we propose adaptive pilot-aware local combining strategies, generalized PFZF (G-PFZF) and generalized PWPFZF (G-PWPFZF), that dynamically allocate spatial degrees of freedom based on local channel conditions and replace heuristic grouping with a decentralized pilot-level optimization framework. Thus providing substantial performance gains over conventional PFZF and PWPFZF. Further, centralized decoding has recently emerged as a promising technique for interference suppression in D-mMIMO systems. However, it incurs substantial fronthaul overhead and computational costs. We develop a decentralized large-scale fading decoding (d-LSFD) scheme in which each AP computes LSFD weights using only locally available channel statistics. We derive a lower bound on the signal-to-interference-plus-noise ratio that explicitly quantifies the performance gap between the proposed d-LSFD scheme and centralized LSFD (c-LSFD), and identifies conditions under which the proposed decentralized solution approaches the centralized optimum. Numerical results demonstrate that the proposed generalized combining and the d-LSFD scheme together achieve significantly higher sum spectral efficiency in comparison to any combination of existing local combining and decoding schemes, while also substantially reducing the computational cost and fronthaul overhead.

Index Terms

Distributed Massive MIMO, Zero-forcing Combining, Spectral Efficiency, Distributed Decoding

I. INTRODUCTION

DISTRIBUTED massive MIMO (D-mMIMO) systems have emerged as a promising architecture for next-generation wireless systems, as they can provide uniform service quality across the network by enabling numerous distributed access points (APs) to coherently serve user equipments (UEs) [1], [2]. However, achieving scalable signal processing in uplink D-mMIMO systems remains challenging because centralized processing architectures require significant fronthaul signaling and computational overhead [3], [4].

Several centralized and partially centralized combining architectures have been proposed to mitigate inter-user interference in D-mMIMO systems by jointly processing signals or channel statistics across multiple APs. [3], [5]–[10]. While these approaches can achieve strong interference suppression, they require the central processing unit (CPU) to collect signals or channel statistics from multiple APs, resulting in substantial fronthaul overhead and computational costs, as shown in Fig. 1(a). To reduce such costs, a two-layer decoding architecture has been proposed in [1], [3], [8], where each AP performs local combining while the CPU performs a second-stage decoding. Consequently, the overall performance of D-mMIMO systems critically depends on: the design of efficient local combining schemes at the APs and the design of scalable second-stage decoding techniques at the CPU. Local maximum ratio (MR) combining [1], offers low computational complexity, but suffers from limited interference suppression capability. The local partial minimum mean square error (LP-MMSE) combining scheme [3], [8], achieves better interference suppression and performance. However, it does not provide tractable closed-form spectral efficiency (SE) expressions, making system-level analysis and optimization challenging.

To address these limitations of the MR and LP-MMSE combining, recent local combining schemes such as full-pilot ZF (FZF), partial FZF (PFZF), and protected weak PFZF (PWPFZF) [11], [14], exploit the structure of pilot reuse to construct combining vectors that partially suppress interference while retaining analytical tractability. In these schemes, each AP classifies the UEs into strong and weak groups using large-scale fading thresholds, allowing some spatial degrees of freedom to be allocated for interference suppression while preserving array gain for weaker users. Although these schemes provide better interference suppression compared to the MR combining, their user grouping decisions rely on heuristic threshold-based rules. As a result, the number of spatial degrees of freedom allocated for interference mitigation is fixed by predetermined thresholds rather than being adapted to the local channel and interference conditions at each AP.

To address such shortcomings of these zero-forcing schemes, we propose adaptive pilot-level combining strategies that dynamically allocate spatial degrees of freedom based on locally observed channel conditions. Specifically, we introduce two generalized combining schemes, referred to as generalized PFZF (G-PFZF) and generalized PWPFZF (G-PWPFZF). Since users sharing the same pilot cannot be fully distinguished by an AP, grouping decisions are naturally performed at the pilot-level rather than at the user level. Here, each AP independently partitions its set of pilots into strong and weak groups by solving a local sum SE optimization problem. Assigning a pilot to the strong group dedicates a spatial degree of freedom (DoF) to mitigate interference via ZF combining, whereas assigning a pilot to the weak group preserves that DoF for signal enhancement through MR combining. This pilot-level formulation allows each AP to adaptively operate across a range of combining strategies from pure MR to FZF. Performance evaluation of the proposed G-PFZF and G-PWPFZF combining schemes establishes that they significantly outperform PFZF and PWPFZF by enabling adaptive pilot-level allocation of spatial degrees of freedom.

In addition to efficient local combining, scalable second-stage decoding is essential for practical uplink processing in D-mMIMO systems. In [1], [3], the authors have proposed a simple decoding technique, as shown in Fig. 1(c) which suffers from suboptimal interference suppression performance. This motivates the use of centralized large-scale fading decoding (c-LSFD) [8], [11], which exploits large-scale channel statistics to mitigate inter-user

interference across APs, as shown in Fig. 1(b). While user-centric or scalable architectures reduce fronthaul signaling by limiting the set of serving APs for each UE, centralized LSFD (c-LSFD) designs still require the exchange of channel statistics among these APs.

In the optimal c-LSFD scheme [8], [11], each AP forwards both channel statistics and locally detected signals to the CPU, which computes LSFD weights to suppress inter-user interference. However, this approach requires the exchange of large-scale channel statistics and matrix inversions whose dimensions grow with the number of UEs. Partial LSFD (p-LSFD) has been proposed to reduce the processing complexity by considering only dominant interference terms [8], [12]. Nevertheless, p-LSFD still requires centralized decoding and matrix inversions at the CPU. As the network size and user density increase, centralized operations become increasingly expensive in terms of both fronthaul signaling and computational costs, limiting the scalability of the p-LSFD scheme.

To overcome these scalability limitations, a decentralized decoding scheme, as shown in Fig. 1(d), has been proposed in which each AP locally computes decoding weights [13]. This decentralized heuristic LSFD (h-LSFD) scheme relies on heuristic weight selection and does not provide theoretical guarantees on their performance relative to c-LSFD and p-LSFD. Consequently, it remains unclear whether decentralized decoding with h-LSFD can achieve near c-LSFD performance using only locally computable weights without exchanging global channel statistics.

To address this, we propose a principled d-LSFD scheme where each AP computes decoding weights using only locally available channel statistics through a diagonal approximation of the interference covariance matrix. We establish a theoretical connection between c-LSFD and d-LSFD by deriving an explicit SINR bound that quantifies the performance loss due to decentralization. Furthermore, we show that the effectiveness of the proposed d-LSFD scheme is intrinsically linked to the structure of the local combining scheme. It achieves near-optimal performance for combiners that yield a diagonally dominant large-scale interference covariance matrix (e.g., MR/ZF-based), and larger performance gap for combiners with strong global coupling, such as MMSE.

Extensive numerical results demonstrate that the combination of the proposed G-PFZF and G-PWPFZF combining schemes and the proposed d-LSFD scheme, achieves significantly higher sum SE and per-user SE, and substantially reduced computational cost and fronthaul signaling compared to any combination of existing combining schemes and LSFD schemes. These results highlight the effectiveness of combining adaptive pilot-level interference management with d-LSFD for scalable uplink processing in D-mMIMO systems.

A. Contributions

We address the twin challenges of designing effective local combining and scalable decoding by developing adaptive pilot-level combining schemes and a decentralized LSFD scheme. In particular, our main contributions are as follows:

Adaptive Combining Schemes: We propose generalized PFZF (G-PFZF) and generalized PWPFZF (G-PWPFZF) schemes that replace heuristic user-level grouping with a pilot-level spatial DoF allocation and provide an explicit mapping between pilot grouping decisions and the number of spatial degrees of freedom used for interference suppression.

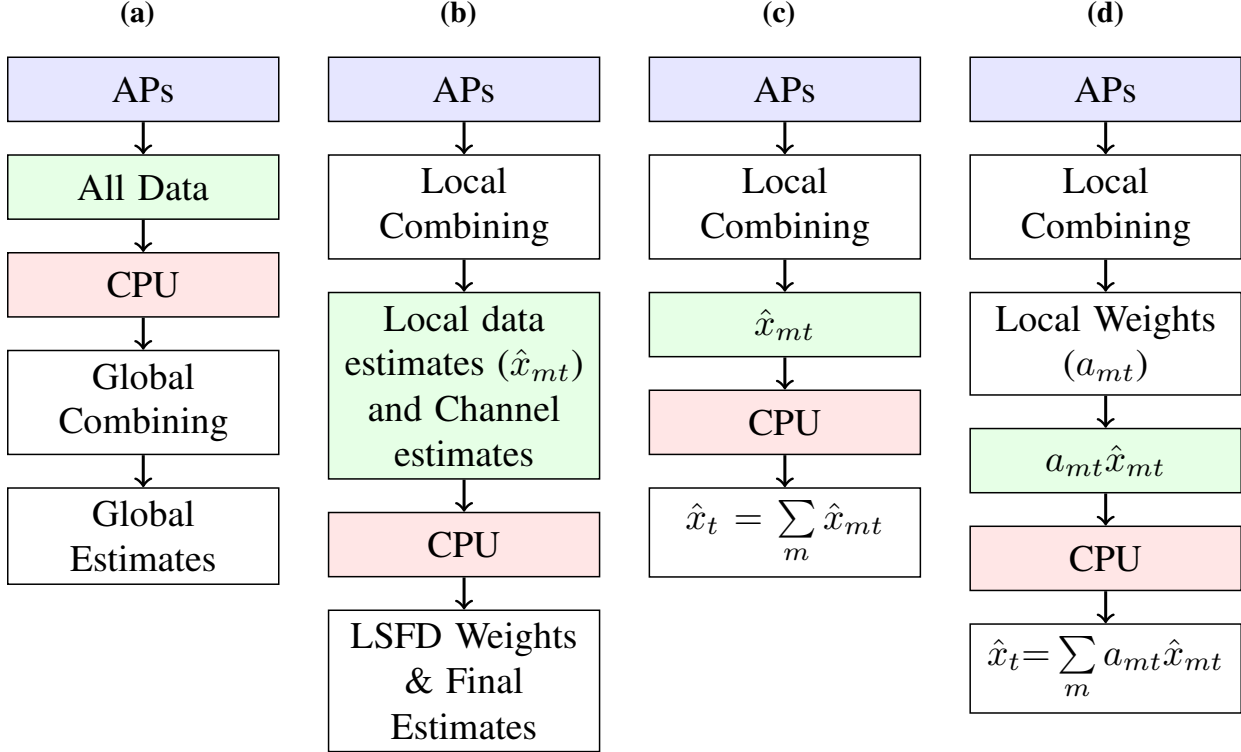


Fig. 1. Uplink processing architectures: (a) Fully centralized, (b) LSFDF with coordination, (c) Simple decoding, (d) Decentralized decoding.

Decentralized LSFDF Scheme: We propose a decentralized-LSFDF (D-LSFDF) scheme where each AP computes decoding weights using only locally available channel statistics. We derive locally computable d-LSFDF weights and establish an explicit SINR bound that quantifies the performance gap between d-LSFDF and c-LSFDF. The analysis further reveals that d-LSFDF is particularly effective for combining schemes that yield diagonally dominant interference covariance matrices, such as ZF- and MR-type combiners.

Closed-form Expressions: Closed-form SINR and corresponding d-LSFDF weights expressions are derived for the proposed combining schemes.

Performance Analysis: Extensive numerical results demonstrate that the combination of the proposed G-PFZF/G-PWPFZF combining and the proposed d-LSFDF outperforms any combination of traditional combining schemes with existing LSFDF schemes by a significant margin, while significantly reducing the computation cost and fronthaul overhead.

Organization: The remainder of the paper is organized as follows. Section II describes the system model, along with the channel estimation and data detection procedures. Section III presents the proposed combining schemes and derives their corresponding closed-form expressions. Section IV provides a rigorous performance evaluation. Finally, Section V concludes the paper and outlines potential directions for future work.

Notation: Scalars are denoted in italics (e.g., x), vectors by bold lowercase letters (e.g., \mathbf{x}), and matrices by bold uppercase letters (e.g., \mathbf{X}). The transpose and Hermitian transpose are denoted by $(\cdot)^T$ and $(\cdot)^H$, respectively, while the complex conjugate is written as $(\cdot)^*$. The sets of real and complex numbers are denoted by \mathbb{R} and \mathbb{C} . The

expectation operator is denoted by $\mathbb{E}[\cdot]$. The size N identity matrix is denoted by \mathbf{I}_N . A complex Gaussian random vector \mathbf{x} with mean $\boldsymbol{\mu}$ and covariance matrix \mathbf{K} is denoted as $\mathbf{x} \sim \mathcal{CN}(\boldsymbol{\mu}, \mathbf{K})$. Also, $[\cdot]_l$ represent the l -th element of the vector $[\cdot]$.

II. SYSTEM MODEL

The system consists of T UEs with a single antenna and M APs, where each AP has A antennas. Within the coverage area of interest, there is a uniform distribution of both APs and UEs, and APs serve the UEs using the same frequency and time resources. The wireless channel follows a block fading model with a coherence block of length L_c symbols, of which L_p symbols are allocated for pilot training. The small-scale fading is represented by a Rayleigh fading vector $\mathbf{h}_{mt} \in \mathbb{C}^{A \times 1}$, and the large-scale fading coefficient (LSFC), encompassing both path-loss and shadowing effects, is denoted by β_{mt} . The channel vector between AP m and UE t , encompassing both small- and large-scale fading, is defined as $\mathbf{g}_{mt} = \beta_{mt}^{1/2} \mathbf{h}_{mt} \in \mathbb{C}^{A \times 1}$. We assume that $\mathbf{h}_{mt} \sim \mathcal{CN}(0, \mathbf{I}_A)$, for all m and t , is an independent and identically distributed (i.i.d) complex Gaussian random vector, thus $\mathbf{g}_{mt} \sim \mathcal{CN}(0, \beta_{mt} \mathbf{I}_A)$. To enhance scalability, we consider user-centric design [8], where \mathcal{T}_m represents the set of UEs served by AP m and \mathcal{M}_t represents the set of APs that are serving UE t .

A. Channel Estimation

A pilot $\sqrt{L_p} \boldsymbol{\psi}_{i_t} \in \mathbb{C}^{L_p \times 1}$ is transmitted by each UE t during the uplink training stage, with $|\boldsymbol{\psi}_{i_t}|^2 = 1$, where i_t is the pilot index of UE t . At the m -th AP, the received signal is:

$$\mathbf{y}_m^{pilot} = \sum_{t=1}^T \sqrt{p_t^p L_p} \mathbf{g}_{mt} \boldsymbol{\psi}_{i_t}^H + \mathbf{N}_m,$$

where $\mathbf{N}_m \in \mathbb{C}^{A \times L_p}$ represents the additive white Gaussian noise (AWGN) matrix characterized by i.i.d. complex Gaussian entries. Additionally, p_t^p represents the normalized pilot power for UE t during pilot transmission. The MMSE estimate of the true channel vector \mathbf{g}_{mt} is provided by [1]:

$$\hat{\mathbf{g}}_{mt} = \sqrt{p_t^p L_p} \beta_{mt} \theta_{mi_t}^{-1} \mathbf{y}_m^{pilot} \boldsymbol{\psi}_{i_t}, \quad (1)$$

where $\theta_{mi_t} = (\sum_{k=1}^T p_k^p L_p \beta_{mk} |\boldsymbol{\psi}_{i_t}^H \boldsymbol{\psi}_{i_k}|^2 + 1)$. The estimate $\hat{\mathbf{g}}_{mt}$ and estimated error $\tilde{\mathbf{g}}_{mt} = \mathbf{g}_{mt} - \hat{\mathbf{g}}_{mt}$ are independent Gaussian with distributions $\hat{\mathbf{g}}_{mt} \sim \mathcal{CN}(0, \gamma_{mt} \mathbf{I}_A)$ and $\tilde{\mathbf{g}}_{mt} \sim \mathcal{CN}(0, (\beta_{mt} - \gamma_{mt}) \mathbf{I}_A)$, where

$$\gamma_{mt} = \mathbb{E}\{|\hat{\mathbf{g}}_{mt}|^2\} = p_t^p L_p \beta_{mt}^2 \theta_{mi_t}^{-1}, \quad (2)$$

Remark 1: The channel estimates of UEs sharing the same pilot sequence are linearly dependent. As a result, an AP cannot fully distinguish among these UEs, leading to residual pilot contamination.

The channel estimates matrix at AP m is denoted by $\hat{\mathbf{G}}_m = [\hat{\mathbf{g}}_{m1}, \hat{\mathbf{g}}_{m2}, \dots, \hat{\mathbf{g}}_{mT}] \in \mathbb{C}^{A \times T}$. Owing to pilot reuse, the columns of $\hat{\mathbf{G}}_m$ exhibit linear dependence, rendering the matrix $\hat{\mathbf{G}}_m$ rank-deficient. The full rank matrix is designed by removing the linearly dependent columns and by including only those columns that contain linearly

independent channel estimates, representing one vector for each pilot sequence. Thus, the matrix $\bar{\mathbf{G}}_m$ is designed as:

$$\bar{\mathbf{G}}_m = \mathbf{y}_m^{pilot} \mathbf{\Psi}, \quad \in \mathbb{C}^{A \times L_p}$$

where $\mathbf{\Psi} = [\boldsymbol{\psi}_1, \boldsymbol{\psi}_2, \dots, \boldsymbol{\psi}_{L_p}]$. Then $\hat{\mathbf{g}}_{mt} = c_{mt} \bar{\mathbf{G}}_m \mathbf{e}_{i_t}$, where \mathbf{e}_{i_t} is the i_t -th column of identity matrix \mathbf{I}_{L_p} .

B. Uplink Transmission and Spectral Efficiency

Let x_t denote the unit power uplink data signal transmitted by UE t . The uplink normalised data power corresponding to UE t and AWGN vector are denoted by p_t^u and $\mathbf{n}_m \sim \mathcal{N}_{\mathbb{C}}(0, \mathbf{I}_A)$, respectively. The signal received at AP m

$$\mathbf{y}_m = \sum_{t=1}^T \mathbf{g}_{mt} \sqrt{p_t^u} x_t + \mathbf{n}_m.$$

In decentralized data detection, each AP performs data detection for its served UEs using a local linear received combining vector and also each AP computes its own interference-suppressing local weight based on the local signal-to-interference-plus-noise ratio (SINR). These weights are applied to the locally detected data symbols before being sent to the CPU. This differs from c-LSFD, where local data and channel estimates are transmitted to the CPU for centralized processing. The locally weighted data symbol \hat{x}_{mt} for UE t at AP m is given by

$$\hat{x}_{mt} = a_{mt} \mathbf{v}_{mt}^H \mathbf{y}_m, \quad (3)$$

where $\mathbf{v}_{mt} \in \mathbb{C}^{A \times 1}$ denotes the local combining vector for UE t at AP m , and a_{mt} is the corresponding decoding weight. These weighted estimates are forwarded to the CPU, which aggregates them to obtain the final estimate of x_t :

$$\hat{x}_t = \sum_{m \in \mathcal{M}_t} a_{mt} \mathbf{v}_{mt}^H \mathbf{y}_m. \quad (4)$$

After expanding \mathbf{y}_m , the (4) can also be rewritten as

$$\begin{aligned} \hat{x}_t &= \sum_{m \in \mathcal{M}_t} \sqrt{p_t^u} a_{mt} \mathbf{v}_{mt}^H \hat{\mathbf{g}}_{mt} x_t + \sum_{m \in \mathcal{M}_t} \sqrt{p_t^u} a_{mt} \mathbf{v}_{mt}^H \tilde{\mathbf{g}}_{mt} x_t \\ &+ \sum_{\substack{k=1 \\ k \neq t}}^T \sum_{m \in \mathcal{M}_t} \sqrt{p_k^u} a_{mt} \mathbf{v}_{mt}^H \mathbf{g}_{mk} x_k + \sum_{m \in \mathcal{M}_t} a_{mt} \mathbf{v}_{mt}^H \mathbf{n}_m. \end{aligned} \quad (5)$$

Based on (5), the achievable uplink SE is obtained using the bounding technique and the corresponding Shannon capacity lower bound [15]–[17] is given by Theorem 1.

Theorem 1 [11], [17]: A lower bound on the uplink ergodic SE for UE t is given by

$$\text{SE}_t^u = L_u \log_2 (1 + \text{SINR}_t), \quad (6)$$

where $L_u = \left(\frac{1 - \frac{L_p}{L_c}}{2}\right)$ and SINR_t is

$$\text{SINR}_t = \frac{p_t^u |\mathbf{DS}_t|^2}{\sum_{k=1}^T p_k^u \mathbb{E}\{|\mathbf{UI}_{tk}|^2\} - p_t^u |\mathbf{DS}_t|^2 + \mathbb{E}\{|\mathbf{GN}_t|^2\}}, \quad (7)$$

$$\begin{aligned} \text{where, } \mathbf{DS}_t &= \sum_{m \in \mathcal{M}_t} a_{mt} \mathbb{E}\{\mathbf{v}_{mt}^H \hat{\mathbf{g}}_{mt}\}, \\ \mathbf{UI}_{tk} &= \sum_{m \in \mathcal{M}_t} a_{mt} \mathbf{v}_{mt}^H \mathbf{g}_{mk}, \\ \mathbf{GN}_t &= \sum_{m \in \mathcal{M}_t} a_{mt} \mathbf{v}_{mt}^H \mathbf{n}_m. \end{aligned}$$

The SE lower bound, in (6), is valid regardless of the combining scheme used.

First, before establishes the relationship between c-LSFD and d-LSFD, we first propose Lemma 1.

Lemma 1 For any $q \geq 0$, define

$$\begin{aligned} F(x, q) &\triangleq \frac{|1+x|^2}{|1+x|^2 + (q - |x|^2)}, \quad x \in \mathbb{C}. \quad \text{Then} \\ \inf_{|x|^2 \leq q} F(x, q) &= \begin{cases} 1 - q, & 0 \leq q < 1, \\ 0, & q \geq 1. \end{cases} \end{aligned}$$

Moreover, for $0 \leq q < 1$, the minimum is attained at $x = -q$, while for $q \geq 1$ the infimum 0 is approached as $x \rightarrow -1$.

Proof: See Appendix B.

The following theorem establishes the relationship between c-LSFD and d-LSFD weights and quantifies the performance loss incurred by decentralization.

Theorem 2 : The c-LSFD weights and the d-LSFD weights that maximize the SE lower bound of UE t are given by $\mathbf{a}_t^o = p_t^u \mathbf{J}_t^{-1} \mathbf{d}_t$ and $\mathbf{a}_t^d = p_t^u \mathbf{D}_t^{-1} \mathbf{d}_t$ respectively, where,

$$\begin{aligned} \mathbf{J}_t &= \sum_{k=1}^T p_k^u \mathbb{E}\{\mathbf{u}_t \mathbf{u}_t^H\} - p_t^u \mathbf{d}_t \mathbf{d}_t^H + \mathbf{F}_t + \tilde{\mathbf{D}}_t, \\ \text{where,} \\ \mathbf{d}_t &= [\mathbb{E}\{\mathbf{v}_{1t}^H \mathbf{g}_{1t}\}, \dots, \mathbb{E}\{\mathbf{v}_{Mt}^H \mathbf{g}_{Mt}\}]^T, \quad \mathbf{u}_{tk} = [\mathbf{v}_{1t}^H \mathbf{g}_{1k}, \dots, \mathbf{v}_{Mt}^H \mathbf{g}_{Mk}]^T \\ \mathbf{F}_t &= \text{diag}\left([\mathbb{E}\{|\mathbf{v}_{1t}^H \mathbf{n}_1|^2\}, \dots, \mathbb{E}\{|\mathbf{v}_{Mt}^H \mathbf{n}_M|^2\}]^T\right). \end{aligned}$$

Here $\mathbf{D}_t = \text{diag}(\mathbf{J}_t)$ and $\tilde{\mathbf{D}}_t \in \mathbb{R}^{M \times M}$ is the diagonal matrix with $[\tilde{\mathbf{D}}_t]_{m,m} = 1$, if $m \notin \mathcal{M}_t$ and zero otherwise. Define $\rho_t \triangleq \frac{\|\mathbf{a}_t^d - \mathbf{a}_t^o\|_2}{\|\mathbf{a}_t^o\|_2}$, and the condition number of \mathbf{J}_t as $\kappa_t \triangleq \frac{\lambda_{\max}(\mathbf{J}_t)}{\lambda_{\min}(\mathbf{J}_t)}$. Then the achievable SINR of d-LSFD satisfies

$$\frac{\text{SINR}_t(\mathbf{a}_t^d)}{\text{SINR}_t(\mathbf{a}_t^o)} \geq \max\{0, 1 - \kappa_t \rho_t^2\}. \quad (8)$$

Proof: See Appendix B.

Remark 2: The bound in (8) shows that the performance gap between d-LSFD and c-LSFD depends on the relative weight mismatch ρ_t and the conditioning of \mathbf{J}_t . In practice, the dominant factor is the mismatch ρ_t , which arises due to local nature of d-LSFD weights. Consequently, d-LSFD approximates the centralized solution, and when ρ_t is small the resulting SINR loss becomes negligible.

The following proposition highlights a special case in which the d-LSFD becomes identical to c-LSFD.

Proposition 1 (Exactness of the bound) : *If the local combining scheme at each AP is either MR or ZF and each UE is assigned an orthogonal pilot sequence ($L_p = T$), then the interference covariance matrix \mathbf{J}_t becomes diagonal. Consequently, the d-LSFD weights coincide with the c-LSFD weights, i.e., $\mathbf{a}_t^d = \mathbf{a}_t^c$, and the SINR bound in Theorem 2 holds with equality.*

Proof: See Appendix C.

Remark 3: For ZF/MR combining, the approximation of d-LSFD depends on pilot contamination as non-diagonal term of \mathbf{J}_t depends on pilot contamination. This implies that lesser the pilot contamination better the approximation.

III. ADAPTIVE COMBINING ANALYSIS

In this section, we focus on G-PFZF and G-PWPFZF schemes that overcome the limitations of threshold-based UE partitioning. For these combining schemes, we derive closed-form expressions for the uplink SE and the corresponding d-LSFD weights.

A. Generalized Partial Full-Pilot Zero-Forcing Combining Scheme

In this work, we propose the G-PFZF combining scheme, in which each AP independently designs combining vectors at the pilot level. Since APs cannot distinguish between individual UEs sharing the same pilot, all UEs associated with the same pilot employ a common pilot-level combining vector. The pilot-level combining design is governed by a local sum spectral efficiency optimization that determines whether each pilot is treated as strong or weak, thereby explicitly controlling the allocation of spatial degrees of freedom between interference suppression and desired signal enhancement. Unlike conventional PFZF, the proposed G-PFZF does not enforce that at least one pilot must be treated as strong, thereby allowing each AP to flexibly operate in MR, PFZF, or full ZF mode depending on local channel and interference condition.

For AP m , let \mathcal{S}_m and \mathcal{W}_m denote the sets of strong and weak pilots, respectively, and let $L_{\mathcal{S}_m}$ be the number of strong pilots. Define the set of strong pilot indices as $\mathcal{R}_{\mathcal{S}_m} = \{r_{m,1}, \dots, r_{m,L_{\mathcal{S}_m}}\}$. Let $\bar{\mathbf{G}}_m \in \mathbb{C}^{A \times L_p}$ collect the estimated channel vectors corresponding to all L_p orthogonal pilots, and define the selection matrix $\mathbf{E}_{\mathcal{S}_m} = [\mathbf{e}_{r_{m,1}}, \dots, \mathbf{e}_{r_{m,L_{\mathcal{S}_m}}}]$. For a given pilot $i \in \mathcal{S}_m$, let $j_{mi} \in \{1, 2, \dots, L_{\mathcal{S}_m}\}$ denote the index of pilot i within $\mathcal{R}_{\mathcal{S}_m}$, and define the vector $\boldsymbol{\varepsilon}_{j_{mi}} \in \mathbb{C}^{L_{\mathcal{S}_m}}$ as the j_{mi} -th column of the identity matrix $\mathbf{I}_{L_{\mathcal{S}_m}}$, such that $\mathbf{E}_{\mathcal{S}_m} \boldsymbol{\varepsilon}_{j_{mi}} = \mathbf{e}_i$. The pseudo-inverse of matrix for ZF structure can be expressed as $(\mathbf{E}_{\mathcal{S}_m}^H \bar{\mathbf{G}}_m^H \bar{\mathbf{G}}_m \mathbf{E}_{\mathcal{S}_m})^{-1}$. To obtain the combining

vector associated with a specific pilot, this pseudo-inverse term is multiplied by $\boldsymbol{\varepsilon}_{j_{mi}}$ and subsequently normalized. Thus, the local ZF vector for pilot $i \in \mathcal{S}_m$ at AP m is given by:

$$\mathbf{v}_{mi}^{\text{LZF}} = \frac{\bar{\mathbf{G}}_m \mathbf{E}_{\mathcal{S}_m} (\mathbf{E}_{\mathcal{S}_m}^H \bar{\mathbf{G}}_m^H \bar{\mathbf{G}}_m \mathbf{E}_{\mathcal{S}_m})^{-1} \boldsymbol{\varepsilon}_{j_{mi}}}{\sqrt{\mathbb{E}\{\|\bar{\mathbf{G}}_m \mathbf{E}_{\mathcal{S}_m} (\mathbf{E}_{\mathcal{S}_m}^H \bar{\mathbf{G}}_m^H \bar{\mathbf{G}}_m \mathbf{E}_{\mathcal{S}_m})^{-1} \boldsymbol{\varepsilon}_{j_{mi}}\|^2\}}}, \quad (9)$$

Similarly, the MR combining vector for pilot $i \in \mathcal{W}_m$ at AP m corresponds directly to the channel vector associated with that pilot and is expressed as:

$$\mathbf{v}_{mi}^{\text{MR}} = \frac{\bar{\mathbf{G}}_m \mathbf{e}_i}{\sqrt{\mathbb{E}\{\|\bar{\mathbf{G}}_m \mathbf{e}_i\|^2\}}} = \frac{\bar{\mathbf{G}}_m \mathbf{e}_i}{\sqrt{A\theta_{mi}}}. \quad (10)$$

Following [18]–[20], the normalization term in (9), for $L_{\mathcal{S}_m} \times L_{\mathcal{S}_m}$ complex Wishart matrix $(\mathbf{E}_{\mathcal{S}_m}^H \bar{\mathbf{G}}_m^H \bar{\mathbf{G}}_m \mathbf{E}_{\mathcal{S}_m})$ with DoF satisfying $A \geq L_{\mathcal{S}_m} + 1$, is

$$\mathbb{E}\{\boldsymbol{\varepsilon}_{j_{mi}}^H (\mathbf{E}_{\mathcal{S}_m}^H \bar{\mathbf{G}}_m^H \bar{\mathbf{G}}_m \mathbf{E}_{\mathcal{S}_m})^{-1} \boldsymbol{\varepsilon}_{j_{mi}}\} = \frac{1}{(A - L_{\mathcal{S}_m})\theta_{mi}}, \quad (11)$$

Also, the G-PFZF scheme suppresses the interference among the UEs whose pilot lies in \mathcal{S}_m by sacrificing $L_{\mathcal{S}_m}$ degrees of freedom from total A degrees to boost the desired signal. Therefore, for any UE t such that $i_t \in \mathcal{S}_m$

$$(\mathbf{v}_{mi_t}^{\text{LZF}})^H \hat{\mathbf{g}}_{mk} = \begin{cases} \sqrt{(A - L_{\mathcal{S}_m})\gamma_{mk}} & \text{if } i_k = i_t, \\ 0, & \text{if } i_k \neq i_t, \end{cases} \quad (12)$$

$$\mathbb{E}\left\{\left|(\mathbf{v}_{mi_t}^{\text{LZF}})^H \hat{\mathbf{g}}_{mk}\right|^2\right\} = \begin{cases} (A - L_{\mathcal{S}_m})\gamma_{mk} & \text{if } i_k = i_t, \\ 0, & \text{if } i_k \neq i_t \text{ and } i_k \in \mathcal{S}_m, \\ \gamma_{mk}, & \text{if } i_k \notin \mathcal{S}_m \end{cases} \quad (13)$$

Similarly, for any UE t such that $i_t \in \mathcal{W}_m$

$$\mathbb{E}\{(\mathbf{v}_{mi_t}^{\text{MR}})^H \hat{\mathbf{g}}_{mk}\} = \begin{cases} \sqrt{A\gamma_{mk}} & \text{if } i_k = i_t, \\ 0, & \text{if } i_k \neq i_t. \end{cases} \quad (14)$$

$$\mathbb{E}\left\{\left|(\mathbf{v}_{mi_t}^{\text{MR}})^H \hat{\mathbf{g}}_{mk}\right|^2\right\} = \begin{cases} (A + 1)\gamma_{mk} & \text{if } i_k = i_t, \\ \gamma_{mk}, & \text{if } i_k \neq i_t, \end{cases} \quad (15)$$

By using the combining vectors in (9) and (10), the closed-form expression of achievable SE for G-PFZF combining can be computed using Theorem 1 with the corresponding SINR given by (16), where \mathcal{P}_{i_t} represents the subset of UEs sharing pilot i_t and δ_{mi_t} is defined as:

$$\delta_{mi_t} = \begin{cases} 1, & \text{if } i_t \in \mathcal{S}_m, \\ 0, & \text{otherwise.} \end{cases} \quad (17)$$

The closed-form expression of d-LSFD weights for UE t at m for G-PFZF combining scheme following the

$$\text{SINR}_t^{\text{G-PFZF}} = \frac{p_t^u \left| \sum_{m \in \mathcal{M}_t} a_{mt} \sqrt{(A - \delta_{mi_t} L_{S_m}) \gamma_{mt}} \right|^2}{\sum_{k \in \mathcal{P}_{i_t} \setminus \{t\}} p_k^u \left| \sum_{m \in \mathcal{M}_t} a_{mt} \sqrt{(A - \delta_{mi_t} L_{S_m}) \gamma_{mk}} \right|^2 + \sum_{k=1}^T p_k^u \sum_{m \in \mathcal{M}_t} |a_{mt}|^2 (\beta_{mk} - \delta_{mi_t} \delta_{mi_k} \gamma_{mk}) + \sum_{m \in \mathcal{M}_t} |a_{mt}|^2} \quad (16)$$

$$\text{SINR}_{mt}^{\text{G-PFZF}} = \frac{S_{mt}}{I_{mt}} = \frac{p_t^u \left(A - \delta_{mi_t} - \delta_{mi_t} \sum_{i=1, i \neq i_t}^{L_p} \delta_{mi} \right) \gamma_{mt}}{\sum_{k \in \mathcal{P}_{i_t} \setminus \{t\}} p_k^u \left(A - \delta_{mi_t} - \delta_{mi_t} \sum_{i=1, i \neq i_t}^{L_p} \delta_{mi} \right) \gamma_{mk} + \sum_{k \in \mathcal{P}_{i_t}} p_k^u (\beta_{mk} - \delta_{mi_t} \gamma_{mk}) + \sum_{k \notin \mathcal{P}_{i_t}} p_k^u (\beta_{mk} - \delta_{mi_t} \delta_{mi_k} \gamma_{mk}) + 1} \quad (19)$$

Theorem 2 for SINR expression in (16) is given by:

$$a_{mt} = \frac{\sqrt{p_t^u (b_{tt}^m)}}{\sum_{k \in \mathcal{P}_{i_t} \setminus \{t\}} p_k^u (b_{kt}^m)^2 + W_{mt}}, \quad (18)$$

where,

$$b_{kt}^m = \sqrt{(A - \delta_{mi_t} L_{S_m}) \gamma_{mk}},$$

$$W_{mt} = \sum_{k=1}^T p_k^u (\beta_{mk} - \delta_{mi_t} \delta_{mi_k} \gamma_{mk}) + 1.$$

The derivation of the closed-form SINR and d-LSFD expressions are given in Appendix D.

Remark 4: In conventional PFZF, UEs are classified as strong or weak using LSFCs thresholds. However, because multiple UEs may share the same pilot, UE-level binary grouping does not yield a unique or explicit mapping to the number of spatial degrees of freedom required for interference suppression. In contrast, pilot-level binary grouping establishes a explicit mapping, allowing the number of required spatial degrees of freedom to be written explicitly as $L_{S_m} = \sum_{i=1}^{L_p} \delta_{mi}$, which is essential for formulating a tractable optimization problem.

Adaptive Pilot Grouping for G-PFZF Combining: This subsection details the local optimization framework that each AP employs to independently partition its set of pilots into strong and weak.

The optimization is based on a local SINR metric derived from the global SINR expression in (16). Specifically, the local SINR of UE t at AP m is obtained by assuming that only AP m contributes to the reception of UE t . Moreover, by substituting $L_{S_m} = \sum_{i=1}^{L_p} \delta_{mi}$, the dependence of the SINR on the pilot-level grouping decision at AP m becomes explicit. This explicit representation is essential, as the pilot grouping variables $\{\delta_{mi}\}$ constitute the optimization variables in the proposed framework. The resulting local SINR expression is given in (19).

Allocating a pilot to the strong group ($\delta_{mi}=1$) assigns a ZF combining vector to that pilot, thereby suppressing coherent interference from UEs sharing the same pilot as well as from UEs associated with other strong pilots. This interference suppression is achieved by consuming one spatial DoF per strong pilot, which reduces the available array gain to $(A - L_{S_m})$ for all UEs served by AP m . Conversely, classifying a pilot as weak preserves the full

array gain but provides no interference suppression for the corresponding UEs. This fundamental trade-off between array gain and interference mitigation makes the pilot grouping problem non-trivial and renders fixed, network-wide threshold-based grouping highly suboptimal. To navigate this trade-off, AP m independently solves a local optimization problem, which is formulated as

$$\max_{\delta_m} \sum_{t=1}^T \log_2 \left(1 + \frac{S_{mt}}{I_{mt}} \right), \quad (20a)$$

$$\text{subject to: } \delta_{mi} \in [0, 1], \forall i, \quad (20b)$$

$$A - 1 \geq \sum_{i=1}^{L_p} \delta_{mi}, \quad (20c)$$

where $\delta_m = [\delta_{m1}, \delta_{m2}, \dots, \delta_{mL_p}]^T$. The constraint (20c) represents the necessary condition of Wishart matrix for interference suppression. Also, intuitively, this would otherwise lead to invalid negative values for the desired signal power and coherent interference in the SINR expression.

The problem in (20) is a Mixed-Integer Non-Linear Program (MINLP), a class of problems known for its exponential computational cost. To develop a more tractable formulation, we begin by relaxing the binary constraint (20b) into a continuous one:

$$0 \leq \delta_{mi} \leq 1, \forall i. \quad (21)$$

To ensure original binary requirement ($\delta_{mi} \in \{0, 1\}$), we introduce the complementary constraint:

$$\delta_{mi} - \delta_{mi}^2 \leq 0, \forall i. \quad (22)$$

The combined constraints (21) and (22) are equivalent to the original binary constraint (20b), as the only values between 0 and 1 that satisfy $\delta_{mi}(1 - \delta_{mi}) \leq 0$ are precisely 0 and 1. Thus, the problem can be written as

$$\max_{\delta_m} \sum_{t=1}^T \log_2 \left(1 + \frac{S_{mt}}{I_{mt}} \right), \quad (23a)$$

$$\text{subject to: (20c), (21), (22).} \quad (23b)$$

Although the problem can be solved using generic non-convex optimization solvers, such approaches become computationally expensive for large networks. Therefore, to solve this problem with low computation cost, we employ gradient based proximal gradient ascent (PGA) method [21], [22]. We first reformulate the problem as:

$$\max_{\delta_m} f(\delta_m), \quad (24a)$$

$$\text{subject to: (21), where,} \quad (24b)$$

$$f(\boldsymbol{\delta}_m) = \sum_{t=1}^T \log_2 \left(1 + \frac{S_{mt}}{I_{mt}} \right) - \chi \left(\lambda_1 \sum_{i=1}^{L_p} \max \left(0, \delta_{mi} - \delta_{mi}^2 \right)^2 + \lambda_2 \max \left(0, \sum_{i=1}^{L_p} \delta_{mi} - A + 1 \right)^2 \right),$$

where χ is a penalty parameter, and λ_1 and λ_2 are weights.

Lemma 2 : *For a sufficiently large penalty χ^* , the solution to Problem (24) is equivalent to the solution of Problem (23).*

Proof: As $\chi \rightarrow +\infty$, the penalty terms $\chi\lambda_1$ and $\chi\lambda_2$ enforce that any constraint violation is driven to zero for the solution to remain finite. Given that the original problem's feasible set is bounded (as argued in [23, Proposition 1]), there exists a finite χ^* such that the solutions coincide.

For practical consideration, the penalty function should be sufficiently small ($\leq 10^{-3}$), for some value of χ . In our numerical simulations, we initialize $\chi=1$ with $\lambda_1=5$ and $\lambda_2=10$ to ensure sufficiently small penalty function [22].

To solve Problem (24) using the PGA method at each AP independently, we follow the steps outlined in Algorithm 1. We initialize $\boldsymbol{\delta}_m$ and update it along with the gradient ascent direction of $f(\boldsymbol{\delta}_m^{(j)})$ with step size α , followed by projection onto $[0, 1]$ to satisfy the box constraint (21):

$$\boldsymbol{\delta}_m^{(j+1)} = \text{proj}_{[0,1]} \left(\boldsymbol{\delta}_m^{(j)} + \alpha \nabla f(\boldsymbol{\delta}_m^{(j)}) \right). \quad (25)$$

The components of gradient $\nabla f(\boldsymbol{\delta}_m)$ can be written as

$$\begin{aligned} \frac{\partial f(\boldsymbol{\delta}_m)}{\partial \delta_{mi}} &= \sum_{t=1}^T \frac{I_{mt}}{I_{mt} + S_{mt}} \frac{I_{mt} \frac{\partial S_{mt}}{\partial \delta_{mi}} - S_{mt} \frac{\partial I_{mt}}{\partial \delta_{mi}}}{I_{mt}^2} \\ &\quad - \chi \left(2\lambda_1 \max \left(0, \delta_{mi} - \delta_{mi}^2 \right) \left(1 - 2\delta_{mi} \right) \right. \\ &\quad \left. + 2\lambda_2 \max \left(0, \sum_{j=1}^{L_p} \delta_{mj} - A + 1 \right) \right), \end{aligned} \quad (26)$$

where

$$\begin{aligned} \frac{\partial S_{mt}}{\partial \delta_{mi}} &= \begin{cases} -p_t^u \left(1 + \sum_{j=1, j \neq i_t}^{L_p} \delta_{mj} \right) \gamma_{mt}, & \text{if } i_t = i, \\ -p_t^u \delta_{mi_t} \gamma_{mt}, & \text{if } i_t \neq i, \end{cases} \\ \frac{\partial I_{mt}}{\partial \delta_{mi}} &= \begin{cases} -\sum_{k \in \mathcal{P}_{i_t} \setminus \{t\}} p_k^u \left(1 + \sum_{j=1, j \neq i_t}^{L_p} \delta_{mj} \right) \gamma_{mk} - \sum_{k \in \mathcal{P}_{i_t}} p_k^u \gamma_{mk}, & \text{if } i_t = i, \\ -\sum_{k \in \mathcal{P}_{i_t} \setminus \{t\}} p_k^u \delta_{mi_t} \gamma_{mk} - \sum_{k \in \mathcal{P}_{i_t}} p_k^u \delta_{mi_t} \gamma_{mk}, & \text{if } i_t \neq i, \end{cases} \end{aligned}$$

Algorithm 1 Proximal Gradient Ascent (PGA) Method

```

1: for all  $m \in \mathcal{M}$  independently do
2:   Initialize:  $j = 1, k = 1, \delta_m^{(1)}, s^{(k)} = f(\delta_m^{(1)}), \chi = 1, \Delta > 1, \epsilon = 5e^{-3}$ 
3:   repeat
4:     repeat
5:       Compute:
6:          $\delta_m^{(j+1)} = \min(1, \max(0, \delta_m^{(j)} + \alpha \nabla f(\delta_m^{(j)})))$ 
7:       Update  $j = j + 1$ 
8:       until  $\left| \frac{f(\delta_m^{(j)}) - f(\delta_m^{(j-1)})}{f(\delta_m^{(j-1)})} \right| \leq \epsilon$ 
9:       Update  $\chi = \chi \times \Delta, k = k + 1$  and  $s^{(k)} = f(\delta_m^{(j)})$ 
10:      until  $\left| \frac{s^{(k)} - s^{(k-1)}}{s^{(k-1)}} \right| \leq \epsilon$ 
11:   end for

```

B. Generalized Protected Weak Partial Full-Pilot Zero-Forcing Combining Scheme

In this framework, the combiners for all UEs, whether assigned to a strong or weak pilot, are designed to actively suppress interference from all UEs that have a strong pilot. This is achieved by projecting the combining vectors for weak UEs onto the orthogonal complement of the subspace spanned by the strong UEs' effective channels. Consequently, the G-PWPFZF scheme provides universal protection against the most significant sources of interference, improving performance for users on weak pilots, at the cost of higher computation in comparison to G-PFZF scheme due to projection matrix computation at the AP.

In the G-PWPFZF scheme, the strong pilot $i \in \mathcal{S}_m$ are assigned with the combining vectors $\mathbf{v}_{mi}^{\text{LFZ}}$ as in (9). The combining vector allocated to pilot $i \in \mathcal{W}_m$ at AP m is the projected MR (PMR) combining vector, and is given by:

$$\mathbf{v}_{mi}^{\text{PMR}} = \frac{1}{\sqrt{(A - L_{\mathcal{S}_m})\theta_{mi}}} \mathbf{B}_m \bar{\mathbf{G}}_m \mathbf{e}_i, \quad (27)$$

where \mathbf{B}_m is a matrix that projects the received signal onto the orthogonal complement of the subspace spanned by the channels of all strong pilots. It is defined as [18]:

$$\mathbf{B}_m = \mathbf{I}_A - \bar{\mathbf{G}}_m \mathbf{E}_{\mathcal{S}_m} (\mathbf{E}_{\mathcal{S}_m}^H \bar{\mathbf{G}}_m^H \bar{\mathbf{G}}_m \mathbf{E}_{\mathcal{S}_m})^{-1} \mathbf{E}_{\mathcal{S}_m}^H \bar{\mathbf{G}}_m^H,$$

The expected value of the effective channel gain for UE t such that $i_t \in \mathcal{W}_m$

$$\mathbb{E}\{(\mathbf{v}_{mi_t}^{\text{PMR}})^H \hat{\mathbf{g}}_{mk}\} = \begin{cases} \sqrt{(A - L_{\mathcal{S}_m})\gamma_{mk}} & \text{if } i_k = i_t, \\ 0, & \text{if } i_k \neq i_t. \end{cases} \quad (28)$$

$$\mathbb{E}\left\{\left|(\mathbf{v}_{mi_t}^{\text{PMR}})^H \hat{\mathbf{g}}_{mk}\right|^2\right\} = \begin{cases} (A - L_{\mathcal{S}_m} + 1)\gamma_{mk} & \text{if } i_k = i_t, \\ 0, & \text{if } i_k \neq i_t \text{ and } i_k \in \mathcal{S}_m, \\ \gamma_{mk}, & \text{if } i_k \neq i_t, \end{cases}$$

These equations confirm that the PMR combiner successfully nullifies interference from all UEs sharing strong pilots $i_k \in \mathcal{S}_m$. By using the combining vector (9) for strong pilot and (27), the closed-form expression for achievable

$$\text{SINR}_t^{\text{G-PWPFZF}} = \frac{p_t^u \left| \sum_{m \in \mathcal{M}_t} a_{mt} \sqrt{(A - L_{S_m}) \gamma_{mt}} \right|^2}{\sum_{k \in \mathcal{P}_{i_t} \setminus \{t\}} p_k^u \left| \sum_{m \in \mathcal{M}_t} a_{mk} \sqrt{(A - L_{S_m}) \gamma_{mk}} \right|^2 + \sum_{k=1}^T p_k^u \sum_{m \in \mathcal{M}_t} |a_{mk}|^2 (\beta_{mk} - \delta_{mi_k} \gamma_{mk}) + \sum_{m \in \mathcal{M}_t} |a_{mt}|^2} \quad (29)$$

SE for G-PWPFZF combining, as in Theorem 1, can be obtained with the SINR given by (29).

The corresponding closed-form expression of d-LSFD weights for UE t at m for G-PWPFZF combining is:

$$a_{mt} = \frac{\sqrt{p_t^u} b_{kt}^m}{\sum_{k \in \mathcal{P}_{i_t} \setminus \{t\}} p_k^u (b_{kt}^m)^2 + W_{mt}}, \quad \text{where,} \quad (30)$$

$$b_{kt}^m = \sqrt{(A - L_{S_m}) \gamma_{mk}},$$

$$W_{mt} = \sum_{k=1}^T p_k^u (\beta_{mk} - \delta_{mi_k} \gamma_{mk}) + 1.$$

The derivation of the closed-form SINR and d-LSFD expressions are given in Appendix E.

Adaptive Pilot Grouping for G-PWPFZF Combining: This subsection discusses the local optimization framework for pilot grouping in the G-PWPFZF scheme. The objective and constraint structure remain identical to those of the G-PFZF scheme. The sole distinction lies in the expression for the local SINR, which forms the foundation of the utility function $f(\delta_m)$ for pilot-grouping. The local SINR for UE t at AP m for G-PWPFZF scheme is $\text{SINR}_{mt}^{\text{G-PWPFZF}} = \frac{S_{mt}}{I_{mt}}$, where

$$S_{mt} = p_t^u \left(A - \sum_{i=1}^{L_p} \delta_{mi} \right) \gamma_{mt}$$

$$I_{mt} = \sum_{k \in \mathcal{P}_{i_t} \setminus \{t\}} p_k^u \left(A - \sum_{i=1}^{L_p} \delta_{mi} \right) \gamma_{mk} + \sum_{k=1}^K p_k^u (\beta_{mk} - \delta_{mi_k} \gamma_{mk}) + 1.$$

Consequently, the optimization algorithm (Algorithm 1) and the overall structure of the gradient $\nabla f(\delta_m)$ remain unchanged. The impact of the different SINR is confined solely to the calculation of the partial derivatives $\frac{\partial S_{mt}}{\partial \delta_{mi}}$ and $\frac{\partial I_{mt}}{\partial \delta_{mi}}$ within the gradient. For the G-PWPFZF scheme, these derivatives are:

$$\frac{\partial S_{mt}}{\partial \delta_{mi}} = -p_t^u \gamma_{mt}, \quad (31)$$

$$\frac{\partial I_{mt}}{\partial \delta_{mi}} = - \sum_{k \in \mathcal{P}_{i_t} \setminus \{t\}} p_k^u \gamma_{mk} - \sum_{k \in \mathcal{P}_i} p_k^u \gamma_{mk}. \quad (32)$$

These expressions replace their G-PFZF counterparts in the gradient calculation step of Algorithm 1. All other steps of the algorithm proceed identically.

Convergence and Computation Cost Analysis of PGA: Since the feasible set defined by the box constraint (21) is bounded and the gradient function $\nabla f(\delta_m)$ is Lipschitz continuous (proved in Appendix F) with constant $L > 0$,

TABLE I
DECODING COMPUTATION AND FRONTHAUL OVERHEAD PER COHERENCE BLOCK

Decoding	Fronthaul	Computation Cost
c-LSFD [17]	$L_u \sum_{m=1}^M \mathcal{T}_m + 2TM$	$\sum_{t=1}^T \mathcal{M}_t ^2 \frac{ \mathcal{P}_{i_t} +2}{2} + \sum_{t=1}^T \mathcal{M}_t T + \sum_{t=1}^T \frac{ \mathcal{M}_t ^3 - \mathcal{M}_t }{3}$
p-LSFD [17]	$L_u \sum_{m=1}^M \mathcal{T}_m + 2TM$	$\sum_{t=1}^T \mathcal{M}_t ^2 \frac{ \mathcal{P}_{i_t} +2}{2} + \sum_{t=1}^T \mathcal{M}_t \mathcal{K}_t + \sum_{t=1}^T \frac{ \mathcal{M}_t ^3 - \mathcal{M}_t }{3}$
d-LSFD	$L_u \sum_{m=1}^M \mathcal{T}_m $	$\sum_{t=1}^T \mathcal{M}_t T + \sum_{t=1}^T \mathcal{M}_t + \sum_{t=1}^T \mathcal{M}_t ^2$

one should choose $\alpha \in (0, 1/L]$ to ensure the convergence of the PGA method [21], [22]. Step size α is selected using backtracking line-search to achieve convergence for Algorithm 1.

At each AP, the computation cost of Algorithm 1 in each iteration depends upon the gradient computation step and is given by $\mathcal{O}(TL_p)$. For both proposed schemes, the average number of PGA iterations per AP is approximately 7, regardless of whether the number of UEs is 50 or 100. This indicates that the convergence speed of PGA is largely insensitive to UE density. The average runtime per AP on a standard laptop equipped with an Intel Core Ultra 7 processor and 16 GB RAM is approximately 0.01 s for 50 UEs and increases to about 0.02–0.03 s for 100 UEs. This increase is mainly due to the higher cost of objective evaluation rather than slower convergence. These results confirm that the proposed PGA-based pilot grouping is computationally efficient and scalable to dense UE deployments.

IV. PERFORMANCE EVALUATION

We consider a network with $M = 100$ APs with $A = 8$ antennas each and $T = 100$ UEs, uniformly distributed in a square area of size 1×1 km². The LSFCs are generated according to the model in [3], incorporating shadow fading with standard deviation of 8 dB. Pilots are assigned using the scalable pilot assignment strategy from [3]. All UEs are assumed to operate at full transmit power of 100 mW. For the baseline PFZF and PWPZF schemes, UE grouping is performed using 90% of total LSFCs received at the AP, as identified via numerical simulation, to provide the best performance. Also \mathcal{K}_t denotes the set of UEs that have atleast one serving AP in common with UE t . To ensure statistical reliability, all reported results are averaged over 500 independent network realizations.

A. Computation cost and Fronthaul cost

We analyze the computational and fronthaul signaling costs of our proposed d-LSFD and combining schemes. The costs are computed following the approach outlined in [8], [12], [17], [18], where only multiplication and division operations are counted, as these dominate the computational load.

Table I compares the fronthaul and computational costs for c-LSFD, p-LSFD and proposed d-LSFD. In c-LSFD and p-LSFD, each AP must transmit both channel estimates and local data estimates to the CPU, resulting in substantial fronthaul overhead. Furthermore, c-LSFD and p-LSFD require computationally expensive matrix operations such as matrix inversion at the CPU. The d-LSFD eliminates these bottlenecks by avoiding centralized decoding entirely, reducing the fronthaul load for sending data estimates only. The computational cost is similarly streamlined by eliminating the matrix inversions required in c-LSFD.

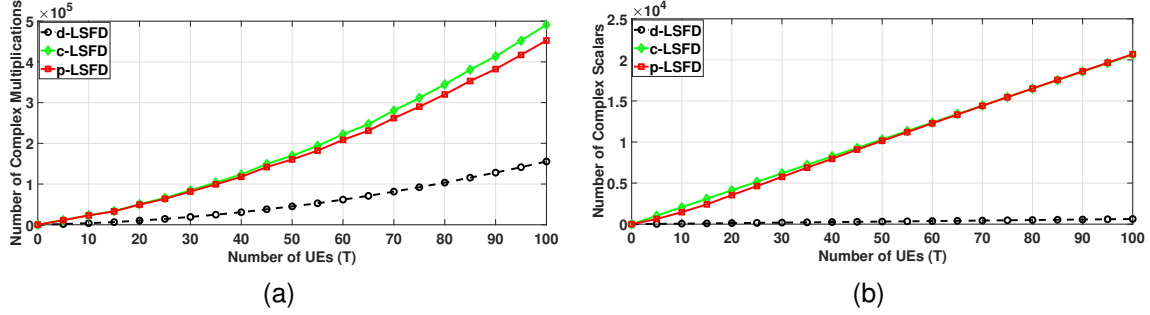


Fig. 2. Comparison of computational and fronthaul costs for different decoding schemes.

TABLE II
COMPUTATIONAL COST PER AP PER COHERENCE BLOCK

Scheme	Combining Vector Computation
PFZF [18]	$\frac{3L_{S_m}^2 A}{2} + \frac{L_{S_m} A}{2} + \frac{L_{S_m}^3 - L_{S_m}}{3} + A \mathcal{T}_m $
G-PFZF	$C_m + AL_p$
PWPFZF [18]	$C_m + 2(L_p - L_{S_m})L_{S_m} A + A \mathcal{T}_m $
G-PWPFZF	$C_m + 2(L_p - L_{S_m})L_{S_m} A + AL_p$

As demonstrated in Fig. 2a, the proposed d-LSFD weights computation provides substantial computation cost reduction compared to c-LSFD, particularly as the number of UEs increases. Similarly, Fig. 2b shows that eliminating channel estimate transmission reduces fronthaul overhead.

The PFZF and PWPFZF schemes exhibit costs that scale linearly with the total number of serving UEs, $|\mathcal{T}_m|$, as shown in Table II. In contrast, the proposed G-PFZF and G-PWPFZF schemes cost scales only with the number of pilots, L_p .

B. Numerical Simulations

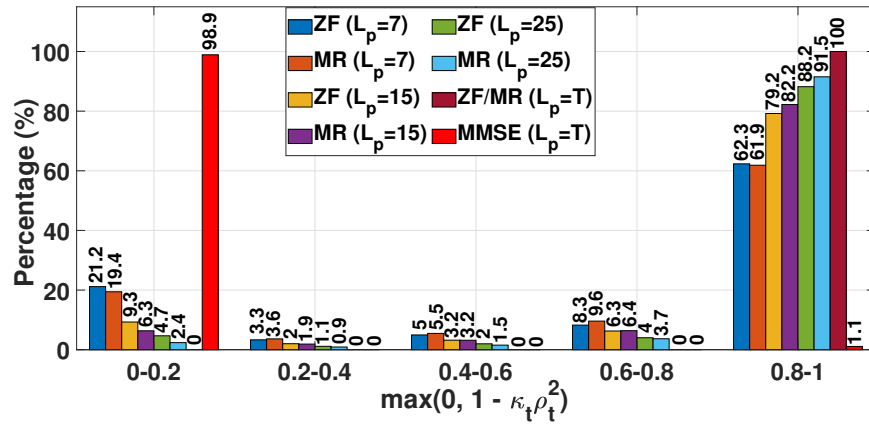


Fig. 3. Empirical distribution versus SINR lower bound in Theorem 2 across different network realizations.

First, we empirically evaluate the tightness of the bound presented in Theorem 2. We also numerically verify Proposition 1 and demonstrate that, for ZF/MR-type combining, the bound is tight and depends on the level of pilot contamination.

Fig. 3 shows the empirical distribution of the bound $\max(0, 1 - \kappa_t \rho_t^2)$ for pilot lengths $L_p \in \{7, 15, 25, T\}$ and for different local combining schemes. For ZF and MR combining, increasing the pilot length shifts the distribution toward the interval 0.8–1, indicating that the d-LSFD solution closely approximates the c-LSFD in most realizations. When $L_p = T$, the bound becomes exactly one for both ZF and MR combining, consistent with Proposition 1. For these schemes, the off-diagonal entries of \mathbf{J}_t are dependent on pilot contamination, which decreases with increase in pilot length, allowing the d-LSFD weights to remain well aligned with the centralized solution.

In contrast, for the MMSE scheme, the bound is concentrated near the interval 0–0.2 even when pilot contamination is removed. This behavior occurs because the MMSE combining vector depends on the channel estimates of all UEs, regardless of whether they share the same pilot sequence. As a result, the off-diagonal entries of the interference matrix \mathbf{J}_t remain significant, and discarding them in the d-LSFD design leads to large deviations from the centralized solution. These results confirm that the proposed d-LSFD scheme is highly effective for ZF/MR-type combining schemes but unsuitable for combiners with strong global coupling, such as MMSE.

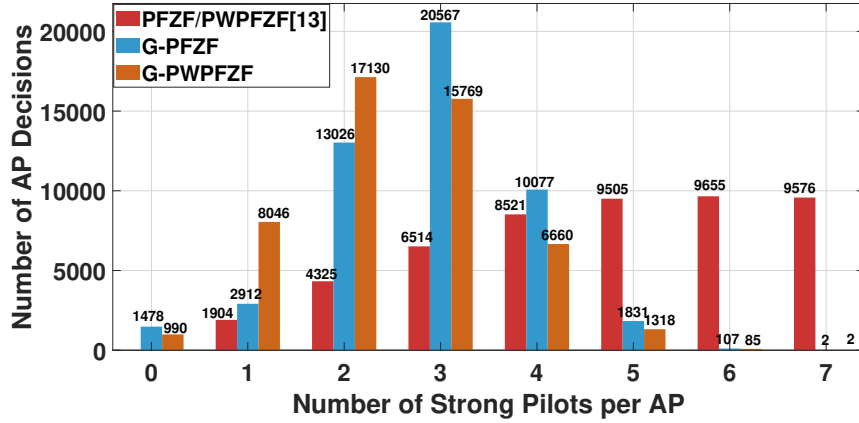


Fig. 4. Distribution of strong pilot decisions.

Fig. 4 shows that the baseline PFZF and PWPFZF schemes exhibit a pronounced peak at $L_{S_m} = 6-7$, revealing their rigid threshold-based strategy that sacrifices excessive degrees of freedom for interference suppression regardless of local conditions. In striking contrast, the proposed G-PFZF and G-PWPFZF schemes show fundamentally different behavior: G-PFZF and G-PWPFZF peaks at 1-4 strong pilots. This efficient allocation preserves spatial resources for signal enhancement. Most notably, the significant non-zero count at $L_{S_m} = 0$ demonstrates our algorithm’s ability to adaptively default to simple MR combining when it is the optimal strategy for a given AP’s local conditions. This demonstrates a seamless, adaptive switching between ZF and MR combining.

Figs. 5 and 6 illustrate the sum SE versus the number of UEs for the proposed G-PFZF and G-PWPFZF combining schemes, respectively, comparing c-LSFD, the proposed d-LSFD, and h-LSFD [13]. For both G-PFZF and G-PWPFZF, the performance gap between d-LSFD and c-LSFD remains consistently within 1–2% across all

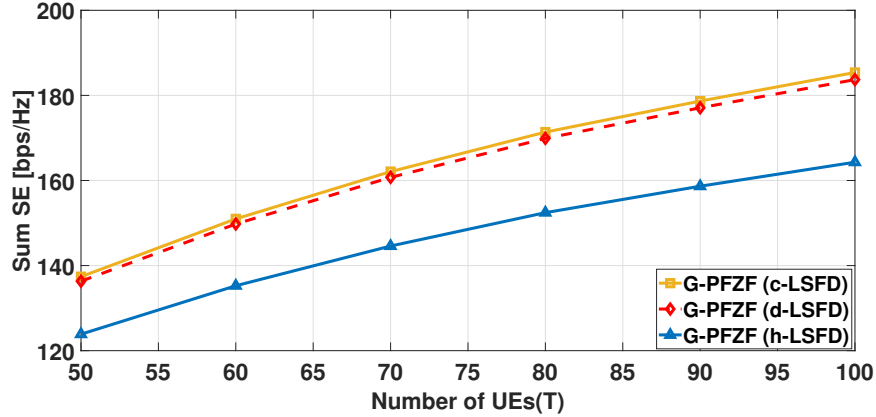


Fig. 5. The uplink sum SE comparison for various decoding schemes.

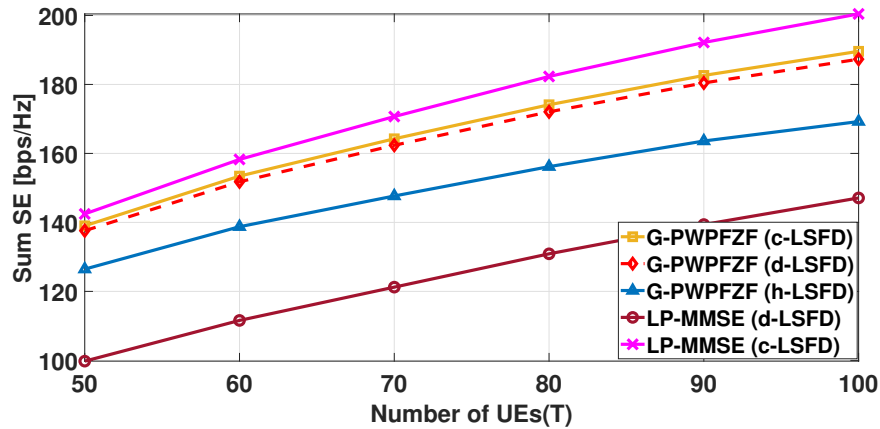


Fig. 6. The uplink sum SE comparison for various decoding schemes.

UE densities. This confirms that the proposed locally computable LSFD weights achieve near-optimal performance within the class of decentralized linear decoders, while completely eliminating the need for network-wide coordination and centralized matrix inversions. In contrast, h-LSFD exhibits a substantially larger performance loss of approximately 10–12%, highlighting the benefit of the proposed principled weight design.

Fig. 6 additionally includes LP-MMSE combining for comparison. While c-LSFD achieves the highest performance for LP-MMSE, the gap between c-LSFD and d-LSFD is very significant. This behavior is consistent with the theoretical analysis in Fig. 3, which shows that the SINR guarantee for d-LSFD becomes vacuous when the ρ_t is large, as is typical for MMSE-based local combining due to strong global interference coupling. These results further validate that the proposed d-LSFD scheme is particularly effective for ZF-type combining schemes.

Fig. 7 illustrates the sum SE versus the number of pilots (L_p), comparing decoding schemes for G-PFZF and G-PWPFZF combining. For G-PFZF and G-PWPFZF combining, the performance gap between d-LSFD and c-LSFD is marginal (less than 3%), when $L_p = 5$, as high pilot contamination makes c-LSFD better equipped to handle interference. However, as the number of pilots increases to moderate values, the gap reduces to negligible. This

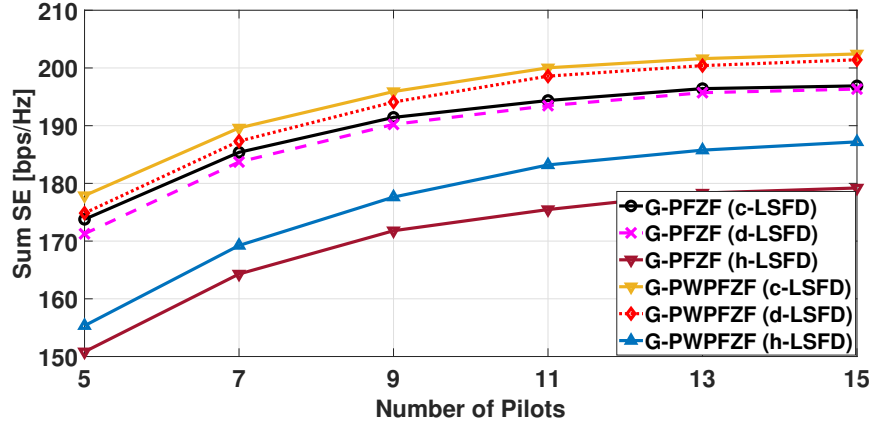


Fig. 7. The uplink sum SE comparison for various decoding schemes.

trend occurs because with sufficient orthogonal pilots, both approaches have similar capability to mitigate pilot contamination. Notably, even in the worst-case scenario with limited number of orthogonal pilots, the performance penalty remains modest, validating that the substantial fronthaul and computation reductions of our d-LSFD approach come with acceptable performance trade-offs across all pilot sequences. Furthermore, the proposed d-LSFD outperform the h-LSFD with a significant margin across all pilot densities for both the combining schemes. These results further show that the proposed d-LSFD retains near-centralized performance, for all pilot densities.

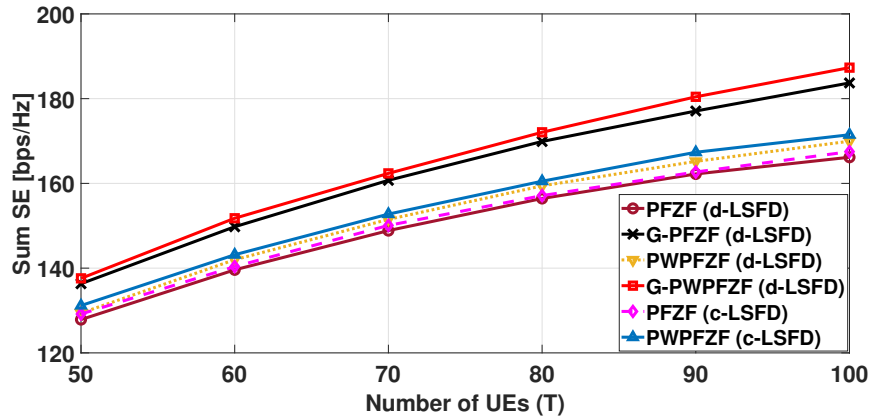


Fig. 8. The uplink sum SE comparison for various combining schemes.

Fig. 8 depicts the sum SE versus the number of UEs (T) for various combining schemes. Compared with the baseline PFZF and PWPFZF schemes, when using either c-LSFD or d-LSFD, the proposed G-PFZF and G-PWPFZF with d-LSFD achieve gains of 6%-9.5% and 5%-10%, respectively, with the gaps widening as the number of UEs increases. This performance improvement comes from the adaptive per-AP pilot classification, which replaces the fixed threshold-based UE grouping of baselines. This enables a more efficient and dynamic trade-off between utilizing degrees of freedom for interference suppression and desired signal enhancement. Consequently, the proposed G-PWPFZF scheme achieves better performance over the G-PFZF scheme by suppressing interference of

the weak UEs from the strong UEs at the APs. By comparing PFZF and PWPZF under both c-LSFD and d-LSFD with their proposed generalized counterparts, the observed performance gains persist irrespective of the decoding strategy. This confirms that the improvements primarily stem from the proposed adaptive pilot-based combining enabled by local optimization.

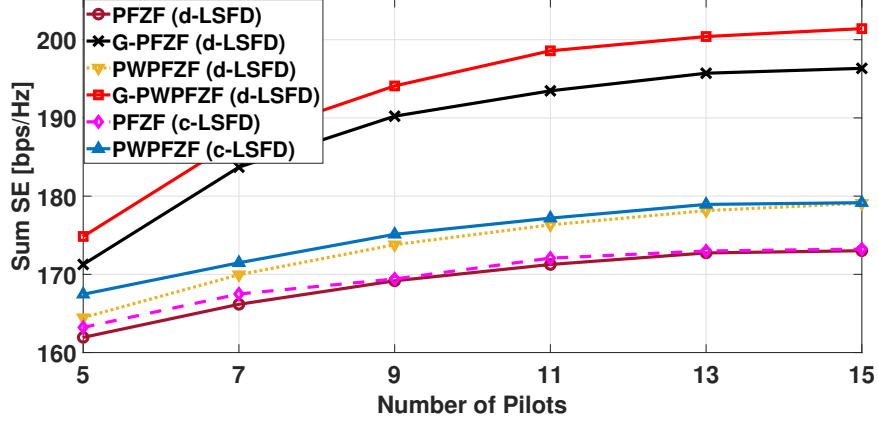


Fig. 9. The uplink sum SE comparison for various combining schemes.

Fig. 9 illustrates the sum SE versus the number of orthogonal pilots L_p , demonstrating the improved performance of the proposed G-PFZF and G-PWPZF with d-LSFD schemes over their respective baseline counterparts with c-LSFD and d-LSFD. The proposed schemes achieve significant performance improvements of 6-14% for G-PFZF and 5-13% for G-PWPZF compared to their respective baselines across different pilot lengths, with the performance gap widening as the number of pilots increases. This expanding gap highlights the advantage of the proposed adaptive pilot grouping strategy over the rigid network-wide threshold approach used in baseline schemes. The baseline schemes must rigidly limit the number of strong pilots to avoid violating the fundamental condition for zero-forcing ($L_{S_m} > A$), which leads to inefficient interference management. In contrast, our proposed decentralized optimization, inherently ensures $L_{S_m} < A$, while maximizing array gain and suppressing interference.

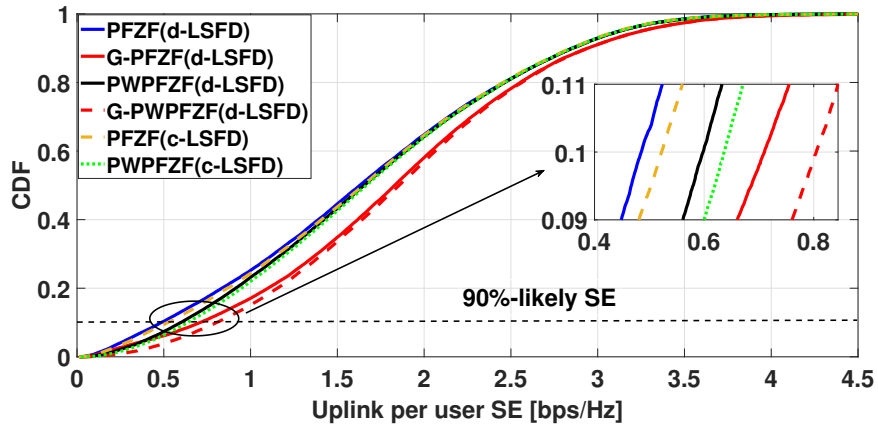


Fig. 10. The uplink SE per user comparison for various combining schemes.

Fig. 10 presents the 90%-likely per-user SE across different combining schemes, demonstrating significant improvements in per user SE through our decentralized optimization framework. The proposed G-PFZF with d-LSFD scheme achieves 40-45% improvement in 90%-likely SE compared to conventional PFZF with both decoding scheme, while G-PWPFZF with d-LSFD shows a 28-34% gain over its baseline PWPFZF across both decoding scheme. These gains confirm that our adaptive per-AP grouping strategy not only enhances the overall system capacity but fundamentally transforms user experience across the network. The gains in 90%-likely SE, particularly, highlight our optimization framework's effectiveness in improving the performance of weak users.

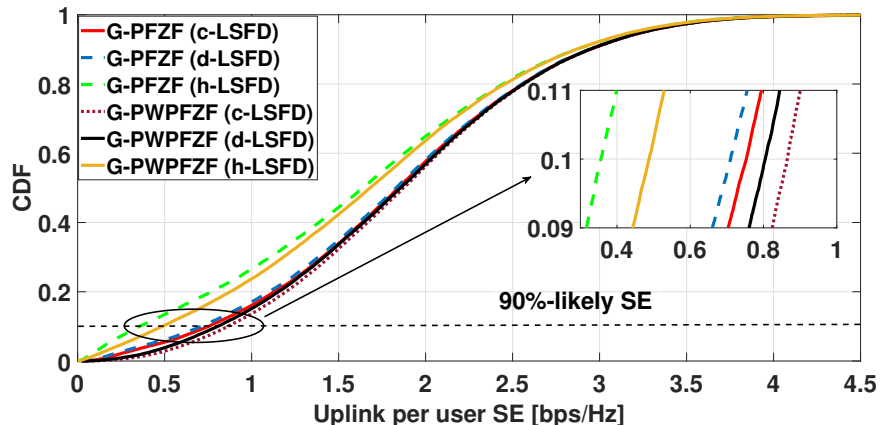


Fig. 11. The uplink SE per user comparison for various decoding schemes.

Fig. 11 presents the 90%-likely per-user SE. While our proposed d-LSFD experience a modest performance reduction of approximately 5.5% and 7% compared to the c-LSFD for G-PFZF and G-PWPFZF scheme respectively. The less than 7% performance difference between d-LSFD and c-LSFD represents a reasonable trade-off for achieving fully decentralized architecture, substantially reduced fronthaul overhead, and lower computational cost. Noticeably, our proposed d-LSFD outperforms the h-LSFD by 100% and 65% for G-PFZF and G-PWPFZF combining respectively, thus outperforming the h-LSFD with significant margin. Overall, the results confirm that near-optimal decentralized decoding and adaptive combining address two orthogonal limitations of existing D-mMIMO systems and jointly enable scalable, high-performance uplink processing.

V. CONCLUSION AND FUTURE WORK

This paper establishes a principled framework for uplink processing in D-mMIMO systems by addressing both local combining and decentralized decoding. We propose two adaptive pilot-aware local combining schemes, G-PFZF and G-PWPFZF, where pilots are partitioned using local optimization. Furthermore, we establish a universal SINR lower bound that rigorously characterizes the performance loss incurred by decentralization of LSFD. A key insight from our theoretical analysis is that the effectiveness of decentralization hinges on the structure of the local combiner. While the proposed d-LSFD is not universally optimal for all combiners, we demonstrate that for the class of pilot-aware ZF-based scheme, it attains near-centralized performance. Numerical results confirmed that, for G-PFZF and G-PWPFZF combining, d-LSFD attains near-optimal performance. In contrast, for LP-MMSE

combining, d-LSFD exhibits a larger performance gap due to the presence of strong global interference coupling. Overall, the proposed framework provides a scalable and theoretically grounded alternative to c-LSFD. In future, we plan to investigate the robustness of generalized combining schemes and the decentralized decoding under hardware impairments.

APPENDIX

A. Proof of Lemma 1

On the domain where $F(x, q)$ is well defined, the denominator is strictly positive. Hence, minimizing $F(x, q)$ over $|x|^2 \leq q$ is equivalent to maximizing

$$G(x) \triangleq \frac{q - |x|^2}{|1 + x|^2}.$$

Write $x = r(\cos \theta + i \sin \theta)$ with $0 \leq r \leq \sqrt{q}$. Then

$$G(r) = \frac{q - r^2}{1 + 2r \cos \theta + r^2}.$$

For fixed r , the $G(r)$ is minimized when $\cos \theta = -1$, yielding

$$G(r) = \frac{q - r^2}{(1 - r)^2}.$$

For $0 \leq q < 1$, the stationary point $r=q$ lies in the admissible interval $[0, \sqrt{q}]$ and gives $G(q) = \frac{q}{1-q}$. Substituting into $F = 1/(1 + G)$ gives

$$\min_{|x|^2 \leq q} F(x, q) = 1 - q.$$

For $q \geq 1$, $G(r)$ can be made arbitrarily large, and therefore

$$\inf_{|x|^2 \leq q} F(x, q) = 0.$$

B. Proof of Theorem 2

$$\text{We know, } \text{SINR}_t(\mathbf{a}_t^\circ) = \frac{|(\mathbf{a}_t^\circ)^H \mathbf{d}_t|^2}{(\mathbf{a}_t^\circ)^H \mathbf{J}_t \mathbf{a}_t^\circ} = (\mathbf{a}_t^\circ)^H \mathbf{J}_t \mathbf{a}_t^\circ > 0.$$

Define the error vector $\boldsymbol{\delta}_t \triangleq \mathbf{a}_t^d - \mathbf{a}_t^\circ$, so that $\mathbf{a}_t^d = \mathbf{a}_t^\circ + \boldsymbol{\delta}_t$ and also $\|\boldsymbol{\delta}_t\|_2 = \rho_t \|\mathbf{a}_t^\circ\|_2$. Using $\mathbf{d}_t = \mathbf{J}_t \mathbf{a}_t^\circ$, define the normalized quantities $x \triangleq \frac{\boldsymbol{\delta}_t^H \mathbf{d}_t}{(\mathbf{a}_t^\circ)^H \mathbf{J}_t \mathbf{a}_t^\circ}$, and $q \triangleq \frac{\boldsymbol{\delta}_t^H \mathbf{J}_t \boldsymbol{\delta}_t}{(\mathbf{a}_t^\circ)^H \mathbf{J}_t \mathbf{a}_t^\circ}$. A direct expansion yields

$$\frac{\text{SINR}_t(\mathbf{a}_t^d)}{\text{SINR}_t(\mathbf{a}_t^\circ)} = \frac{|1 + x|^2}{1 + 2\Re(x) + q}. \quad (\text{T1})$$

By the Rayleigh quotient bounds,

$$q \leq \frac{\lambda_{\max}(\mathbf{J}_t) \|\boldsymbol{\delta}_t\|_2^2}{\lambda_{\min}(\mathbf{J}_t) \|\mathbf{a}_t^\circ\|_2^2} = \kappa_t \rho_t^2,$$

and by the Cauchy-Schwarz inequality in the \mathbf{J}_t -inner product, $|x|^2 \leq q$. Using Lemma 1 for fixed q , we yields

$$\min_{|x|^2 \leq q} \frac{|1+x|^2}{1+2\Re(x)+q} = \max\{0, 1-q\}.$$

Substituting $q \leq \kappa_t \rho_t^2$ completes the proof.

C. Proof of Proposition 1

Consider an off-diagonal entry of \mathbf{J}_t for $m \neq n$:

$$[\mathbf{J}_t]_{mn} = \sum_{k=1, k \neq t}^T p_k^u \mathbb{E} \left\{ \mathbf{v}_{mt}^H \hat{\mathbf{g}}_{mk} \right\} \mathbb{E} \left\{ \mathbf{v}_{nt}^H \hat{\mathbf{g}}_{nk} \right\}.$$

The local MR and ZF combining vectors are linearly dependent only on the channel estimates of UE t and the UEs sharing the same pilot as t , since pilot-sharing UEs have linearly dependent channel estimates as in (1). Hence, for any $k \neq t$ that does not share pilot with t , $\mathbb{E} \left\{ \mathbf{v}_{mt}^H \hat{\mathbf{g}}_{mk} \right\} = 0$, which implies $[\mathbf{J}_t]_{mn} = 0$ for all $m \neq n$. Therefore, \mathbf{J}_t becomes a diagonal matrix.

D. Closed-form SINR and d-LSFD expressions for G-PFZF combining

Pilot-sharing UEs use $\mathbf{v}_{mi_t}^{\text{LZF}}$ for strong pilots and $\mathbf{v}_{mi_t}^{\text{MR}}$ for weak pilots. The desired signal term in (7) can be written as

$$|\text{DS}_t|^2 = \left| \mathbb{E} \left\{ \sum_{m \in \mathcal{Z}_{i_t}} a_{mt} (\mathbf{v}_{mi_t}^{\text{LZF}})^H \hat{\mathbf{g}}_{mt} + \sum_{m \in \mathcal{Y}_{i_t}} a_{mt} (\mathbf{v}_{mi_t}^{\text{MR}})^H \hat{\mathbf{g}}_{mt} \right\} \right|^2,$$

where $\mathcal{Z}_{i_t} \subseteq \mathcal{M}_t$ and $\mathcal{Y}_{i_t} \subseteq \mathcal{M}_t$ denote the subsets of APs where pilot i_t is classified as strong and weak, respectively. Using (12) and (14), the $|\text{DS}_t|^2$ can be written as:

$$\begin{aligned} |\text{DS}_t|^2 &= \left| \sum_{m \in \mathcal{Z}_{i_t}} a_{mt} \sqrt{(A - L_{S_m}) \gamma_{mt}} + \sum_{m \in \mathcal{Y}_{i_t}} a_{mt} \sqrt{A \gamma_{mt}} \right|^2 \\ &= \left| \sum_{m=1}^M a_{mt} \sqrt{(A - \delta_{mi_t} L_{S_m}) \gamma_{mt}} \right|^2, \end{aligned} \tag{A1}$$

The interference term $\mathbb{E} \left\{ |\text{UI}_{tk}|^2 \right\}$ in (7) can be expanded as:

$$\begin{aligned} &\mathbb{E} \left\{ \left| \sum_{m \in \mathcal{Z}_{i_t}} a_{mt} (\mathbf{v}_{mi_t}^{\text{LZF}})^H \mathbf{g}_{mk} + \sum_{m \in \mathcal{Y}_{i_t}} a_{mt} (\mathbf{v}_{mi_t}^{\text{MR}})^H \mathbf{g}_{mk} \right|^2 \right\} \\ &= \mathbb{E} \left\{ \left| \sum_{m \in \mathcal{Z}_{i_t}} a_{mt} (\mathbf{v}_{mi_t}^{\text{LZF}})^H \mathbf{g}_{mk} \right|^2 \right\} + \mathbb{E} \left\{ \left| \sum_{m \in \mathcal{Y}_{i_t}} a_{mt} (\mathbf{v}_{mi_t}^{\text{MR}})^H \mathbf{g}_{mk} \right|^2 \right\} \\ &+ 2 \mathbb{E} \left\{ \sum_{m \in \mathcal{Z}_{i_t}} \sum_{n \in \mathcal{Y}_{i_t}} a_{mt} a_{nt} (\mathbf{v}_{mi_t}^{\text{LZF}})^H \mathbf{g}_{mk} (\mathbf{v}_{ni_t}^{\text{MR}})^H \mathbf{g}_{nk} \right\}. \end{aligned} \tag{A2}$$

The first term (A_1) of (A2) can be rewritten as:

$$\begin{aligned}
A_1 &= \mathbb{E} \left\{ \left| \sum_{m \in \mathcal{Z}_{i_t}} a_{mt} (\mathbf{v}_{mi_t}^{\text{LZF}})^H (\hat{\mathbf{g}}_{mk} + \tilde{\mathbf{g}}_{mk}) \right|^2 \right\} \\
&= \mathbb{E} \left\{ \left| \sum_{m \in \mathcal{Z}_{i_t}} a_{mt} (\mathbf{v}_{mi_t}^{\text{LZF}})^H \hat{\mathbf{g}}_{mk} \right|^2 \right\} + \mathbb{E} \left\{ \left| \sum_{m \in \mathcal{Z}_{i_t}} a_{mt} (\mathbf{v}_{mi_t}^{\text{LZF}})^H \tilde{\mathbf{g}}_{mk} \right|^2 \right\} \\
&= \sum_{m \in \mathcal{Z}_{i_t}} \mathbb{E} \left\{ \left| a_{mt} (\mathbf{v}_{mi_t}^{\text{LZF}})^H \hat{\mathbf{g}}_{mk} \right|^2 \right\} + \left| \sum_{m \in \mathcal{Z}_{i_t}} a_{mt} \mathbb{E} \left\{ (\mathbf{v}_{mi_t}^{\text{LZF}})^H \hat{\mathbf{g}}_{mk} \right\} \right|^2 \\
&\quad - \sum_{m \in \mathcal{Z}_{i_t}} \left| a_{mt} \mathbb{E} \left\{ (\mathbf{v}_{mi_t}^{\text{LZF}})^H \hat{\mathbf{g}}_{mk} \right\} \right|^2 + \sum_{m \in \mathcal{Z}_{i_t}} \mathbb{E} \left\{ \left| (a_{mt} \mathbf{v}_{mi_t}^{\text{LZF}})^H \tilde{\mathbf{g}}_{mk} \right|^2 \right\} \\
&\quad + \left| \sum_{m \in \mathcal{Z}_{i_t}} a_{mt} \mathbb{E} \left\{ (\mathbf{v}_{mi_t}^{\text{LZF}})^H \tilde{\mathbf{g}}_{mk} \right\} \right|^2 - \sum_{m \in \mathcal{Z}_{i_t}} \left| a_{mt} \mathbb{E} \left\{ (\mathbf{v}_{mi_t}^{\text{LZF}})^H \tilde{\mathbf{g}}_{mk} \right\} \right|^2,
\end{aligned}$$

Using (12) and (13), we can rewrite A_1 as

$$\begin{aligned}
A_1 &= \left| \sum_{m \in \mathcal{Z}_{i_t}} a_{mt} \sqrt{(A - L_{S_m}) \gamma_{mk}} \right|^2 |\boldsymbol{\psi}_{i_t}^H \boldsymbol{\psi}_{i_k}|^2 \\
&\quad + \sum_{m \in \mathcal{Z}_{i_t}} |a_{mt}|^2 (\beta_{mk} - \delta_{mi_k} \gamma_{mk}).
\end{aligned} \tag{A3}$$

The second term (A_2) of (A2) is expanded as:

$$\begin{aligned}
A_2 &= \sum_{m \in \mathcal{Y}_{i_t}} \mathbb{E} \left\{ \left| a_{mt} (\mathbf{v}_{mi_t}^{\text{MR}})^H \hat{\mathbf{g}}_{mk} \right|^2 \right\} + \left| \sum_{m \in \mathcal{Y}_{i_t}} a_{mt} \mathbb{E} \left\{ (\mathbf{v}_{mi_t}^{\text{MR}})^H \hat{\mathbf{g}}_{mk} \right\} \right|^2 \\
&\quad - \sum_{m \in \mathcal{Y}_{i_t}} \left| a_{mt} \mathbb{E} \left\{ (\mathbf{v}_{mi_t}^{\text{MR}})^H \hat{\mathbf{g}}_{mk} \right\} \right|^2 + \sum_{m \in \mathcal{Y}_{i_t}} \mathbb{E} \left\{ \left| (a_{mt} \mathbf{v}_{mi_t}^{\text{MR}})^H \tilde{\mathbf{g}}_{mk} \right|^2 \right\} \\
&\quad + \left| \sum_{m \in \mathcal{Y}_{i_t}} a_{mt} \mathbb{E} \left\{ (\mathbf{v}_{mi_t}^{\text{MR}})^H \tilde{\mathbf{g}}_{mk} \right\} \right|^2 - \sum_{m \in \mathcal{Y}_{i_t}} \left| a_{mt} \mathbb{E} \left\{ (\mathbf{v}_{mi_t}^{\text{MR}})^H \tilde{\mathbf{g}}_{mk} \right\} \right|^2,
\end{aligned}$$

Using the (14) and (15), we can rewrite A_2 as

$$A_2 = \left| \sum_{m \in \mathcal{Z}_{i_t}} a_{mt} \sqrt{A \gamma_{mk}} \right|^2 |\boldsymbol{\psi}_{i_t}^H \boldsymbol{\psi}_{i_k}|^2 + \sum_{m \in \mathcal{Z}_{i_t}} |a_{mt}|^2 \beta_{mk}. \tag{A4}$$

Finally, the third term (A_3) of (A2) can be written as:

$$A_3 = 2 \left(\sum_{m \in \mathcal{Z}_{i_t}} a_{mt} \sqrt{(A - L_{S_m}) \gamma_{mt}} \right) \left(\sum_{m \in \mathcal{Y}_{i_t}} a_{mt} \sqrt{A \gamma_{mt}} \right). \tag{A5}$$

Using (A3), (A4) and (A5)

$$\begin{aligned}
\mathbb{E} \left\{ |\mathbf{UI}_{tk}|^2 \right\} &= \left| \sum_{m=1}^M a_{mt} \sqrt{(A - \delta_{mi_t} L_{S_m}) \gamma_{mk}} \right|^2 |\boldsymbol{\psi}_{i_t}^H \boldsymbol{\psi}_{i_k}|^2 \\
&\quad + \sum_{m=1}^M |a_{mt}|^2 (\beta_{mk} - \delta_{mi_t} \delta_{mi_k} \gamma_{mk}).
\end{aligned} \tag{A6}$$

The term $\mathbb{E}\{|GN_t|^2\}$ of interference in (7) can be written as:

$$\begin{aligned} & \sum_{m \in \mathcal{Z}_{i_t}} |a_{mt}|^2 \mathbb{E}\left\{\left|(\mathbf{v}_{mi_t}^{\text{LZF}})^H \mathbf{n}_m\right|^2\right\} + \sum_{m \in \mathcal{Y}_{i_t}} |a_{mt}|^2 \mathbb{E}\left\{\left|(\mathbf{v}_{mi_t}^{\text{MR}})^H \mathbf{n}_m\right|^2\right\} \\ & = \sum_{m=1}^M |a_{mt}|^2 \end{aligned} \quad (\text{A7})$$

Substituting (A1), (A6) and (A7) in (7) gives the (16).

From Theorem 2, the d-LSFD weight for UE t is $\mathbf{a}_t^d = p_t^u \mathbf{D}_t^{-1} \mathbf{d}_t$. Since, \mathbf{D}_t is a diagonal matrix, therefore, the d-LSFD for UE t at AP m can be written as $a_{mt} = p_t^u \frac{[\mathbf{d}_t]_m}{[\mathbf{D}_t]_{mm}}$. Here, the element of \mathbf{d}_t for G-PFZF combining is given by

$$[\mathbf{d}_t]_m = \mathbb{E}\{\mathbf{v}_{mi_t}^H \mathbf{g}_{mt}\} = \sqrt{(A - \delta_{mi_t} L_{S_m}) \gamma_{mt}}.$$

The diagonal element $[\mathbf{D}_t]_{mm}$ is given by

$$\begin{aligned} & \sum_{k=1}^T p_k^u \mathbb{E}\{|\mathbf{v}_{mi_t}^H \mathbf{g}_{mk}|^2\} - p_t^u |\mathbb{E}\{\mathbf{v}_{mi_t}^H \mathbf{g}_{mt}\}|^2 + \mathbb{E}\{|\mathbf{v}_{mi_t}^H \mathbf{n}_m|^2\} \\ & = \sum_{k \in \mathcal{P}_{i_t} \setminus \{t\}} p_k^u \sqrt{(A - \delta_{mi_t} L_{S_m}) \gamma_{mk}} + \sum_{k=1}^T p_k^u (\beta_{mk} - \delta_{mi_t} \delta_{mi_k} \gamma_{mk}) + 1, \end{aligned}$$

where $\mathbf{v}_{mi_t} = \mathbf{v}_{mi_t}^{\text{LZF}}$, if $i_t \in S_m$, and $\mathbf{v}_{mi_t} = \mathbf{v}_{mi_t}^{\text{MR}}$, if $i_t \notin S_m$. These expressions give the d-LSFD weights given in (18).

E. Closed-form SINR and d-LSFD expressions for G-PWPFZF combining

The derivation follows the same steps as in Appendix D, the only difference is that instead of $\mathbf{v}_{mi_t}^{\text{MR}}$, we have $\mathbf{v}_{mi_t}^{\text{PMR}}$ combining vector. The desired signal term in (7)

$$|\text{DS}_t|^2 = \left| \mathbb{E}\left\{ \sum_{m \in \mathcal{Z}_{i_t}} a_{mt} (\mathbf{v}_{mi_t}^{\text{LZF}})^H \hat{\mathbf{g}}_{mt} + \sum_{m \in \mathcal{Y}_{i_t}} a_{mt} (\mathbf{v}_{mi_t}^{\text{PMR}})^H \hat{\mathbf{g}}_{mt} \right\} \right|^2.$$

Using (12) and (28), then

$$|\text{DS}_t|^2 = p_t^u \left| \sum_{m=1}^M a_{mt} \sqrt{(A - L_{S_m}) \gamma_{mk}} \right|^2, \quad (\text{B1})$$

The first term in (7) can be written as

$$\begin{aligned} \mathbb{E}\{|\text{UI}_{tk}|^2\} & = \left| \sum_{m=1}^M a_{mt} \sqrt{(A - L_{S_m}) \gamma_{mk}} \right|^2 |\boldsymbol{\psi}_{i_t}^H \boldsymbol{\psi}_{i_k}|^2 \\ & + \sum_{m=1}^M |a_{mt}|^2 (\beta_{mk} - \delta_{mi_t} \delta_{mi_k} \gamma_{mk}). \end{aligned} \quad (\text{B2})$$

The last term of interference in (7) can be written as:

$$\mathbb{E}\{|GN_t|^2\} = p_k^u \sum_{m=1}^M |a_{mt}|^2 \quad (\text{B3})$$

$$\frac{\partial g(\delta_{mi})}{\partial \delta_{mi}} = \sum_{t=1}^T \left[\frac{(S_{mt} \partial_{\delta_{mi}} I_{mt} - I_{mt} \partial_{\delta_{mi}} S_{mt})(I_{mt} \partial_{\delta_{mi}} S_{mt} - S_{mt} \partial_{\delta_{mi}} I_{mt})}{(I_{mt} + S_{mt})^2 I_{mt}^2} + \frac{I_{mt}}{I_{mt} + S_{mt}} \left(\frac{I_{mt} \partial_{\delta_{mi}}^2 S_{mt} - S_{mt} \partial_{\delta_{mi}}^2 I_{mt}}{I_{mt}^2} \right. \right. \\ \left. \left. - \frac{2 \partial_{\delta_{mi}} I_{mt} (I_{mt} \partial_{\delta_{mi}} S_{mt} - S_{mt} \partial_{\delta_{mi}} I_{mt})}{I_{mt}^3} \right) \right] - \chi \left[2\lambda_1 \mathbf{1}_{\{\delta_{mi} - \delta_{mi}^2 > 0\}} ((1 - 2\delta_{mi})^2 - 2(\delta_{mi} - \delta_{mi}^2)) + 2\lambda_2 \mathbf{1}_{\{2 - A > 0\}} \right]. \quad (\text{C1})$$

Substituting (B1), (B2) and (B3) in (7) gives the (29).

The d-LSFD for UE t at AP m can be written as $a_{mt} = p_t^u \frac{[\mathbf{d}_t]_m}{[\mathbf{D}_t]_{mm}}$, where

$$[\mathbf{d}_t]_m = \sqrt{(A - L_{S_m}) \gamma_{mt}}, \\ [\mathbf{D}_t]_{mm} = \sum_{k \in \mathcal{P}_{it} \setminus \{t\}} p_k^u \sqrt{(A - L_{S_m}) \gamma_{mk}} + \sum_{k=1}^T p_k^u (\beta_{mk} - \delta_{mi_k} \gamma_{mk}) + 1.$$

Here, the weak pilot uses PMR combining vector instead of MR combining vector. The above expression gives the d-LSFD weights in (30).

F. Proof of Lipschitz Continuity of $\nabla f(\boldsymbol{\delta}_m)$

To establish the Lipschitz continuity of $\nabla f(\boldsymbol{\delta}_m)$, we analyze its component functions and their boundedness over the compact domain $\boldsymbol{\delta}_m \in [0, 1]^{L_p}$. The gradient component in (26) is $g(\delta_{mi}) = \frac{\partial f(\boldsymbol{\delta}_m)}{\partial \delta_{mi}}$ bounded as

- $0 < S_{mt}, I_{mt}, \frac{\partial S_{mt}}{\partial \delta_{mi}}, \frac{\partial I_{mt}}{\partial \delta_{mi}} \leq C_1$ (always bounded)
- $\max(0, \delta_{mi} - \delta_{mi}^2) \in [0, \frac{1}{4}]$ (bounded on $[0, 1]$)
- $\max\left(0, \sum_{j=1}^{L_p} \delta_{mj} - A + 1\right) \leq L_p$
- $\frac{I_{mt}}{I_{mt} + S_{mt}} \in (0, 1)$, $C_2 \leq \frac{I_{mt} \frac{\partial S_{mt}}{\partial \delta_{mi}} - S_{mt} \frac{\partial I_{mt}}{\partial \delta_{mi}}}{I_{mt}^2} \leq C_3$,

where C_1, C_2 and C_3 are finite constants. The partial derivatives of $g(\delta_{mi})$ is given by

For all $\delta_{mi} \in [0, 1]$, since all component functions $\frac{\partial g(\delta_{mi})}{\partial \delta_{mi}}$ are bounded and continuously differentiable on the compact domain $[0, 1]^{L_p}$, the Hessian matrix $\nabla^2 f(\boldsymbol{\delta}_m) = \nabla g(\boldsymbol{\delta}_m)$ exists and is continuous. Applying the mean value theorem for vector-valued functions, for any $\mathbf{x}, \mathbf{y} \in [0, 1]^{L_p}$, there exists \mathbf{z} on the line segment between \mathbf{x} and \mathbf{y} such that:

$$\|\nabla f(\mathbf{x}) - \nabla f(\mathbf{y})\| \leq \|\nabla^2 f(\mathbf{z})\|_2 \|\mathbf{x} - \mathbf{y}\| \leq L \|\mathbf{x} - \mathbf{y}\|$$

This establishes the Lipschitz continuity of $\nabla f(\boldsymbol{\delta}_m)$, ensuring convergence of the proximal gradient algorithm.

REFERENCES

- [1] H. Q. Ngo, A. Ashikhmin, H. Yang, E. G. Larsson, and T. L. Marzetta, "Cell-free massive MIMO versus small cells," *IEEE Trans. on Wireless Commun.*, vol. 16, no. 3, pp. 1834–1850, 2017.
- [2] M. S. A. Khan, S. Agnihotri, and R. M. Karthik, "Joint AP-UE association and power factor optimization for distributed massive MIMO," in *Proc. IEEE PIMRC*, Valencia, Spain, Sept. 2024.

- [3] E. Björnson and L. Sanguinetti, "Scalable cell-free massive MIMO systems," *IEEE Trans. on Commun.*, vol. 68, no. 7, pp. 4247–4261, 2020.
- [4] M. S. A. Khan, S. Agnihotri, and R. M. Karthik, "Distributed pilot assignment for distributed massive-MIMO networks," in *Proc, IEEE WCNC*, Dubai, UAE, April 2024.
- [5] D. Maryopi, M. Bashar, and A. Burr, "On the uplink throughput of zero forcing in cell-free massive MIMO with coarse quantization," *IEEE Trans. on Veh. Techno.*, vol. 68, no. 7, pp. 7220–7224, 2019.
- [6] E. Nayebi, A. Ashikhmin, T. L. Marzetta, and B. D. Rao, "Performance of cell-free massive MIMO systems with MMSE and LSFD receivers," in *Proc, IEEE ASILOMAR*, California, USA, Nov. 2016.
- [7] E. Björnson and L. Sanguinetti, "Making cell-free massive MIMO competitive with mmse processing and centralized implementation," *IEEE Trans. on Wireless Commun.*, vol. 19, no. 1, pp. 77–90, 2019.
- [8] Ö. T. Demir, E. Björnson, L. Sanguinetti *et al.*, "Foundations of user-centric cell-free massive MIMO," *Foundations and Trends® in Signal Processing*, vol. 14, no. 3-4, pp. 162–472, 2021.
- [9] L. Du, L. Li, H. Q. Ngo, T. C. Mai, and M. Matthaiou, "Cell-free massive MIMO: Joint maximum-ratio and zero-forcing precoder with power control," *IEEE Trans. on Commun.*, vol. 69, no. 6, pp. 3741–3756, 2021.
- [10] X. Wang, J. Cheng, C. Zhai, and A. Ashikhmin, "Partial cooperative zero-forcing decoding for uplink cell-free massive MIMO," *IEEE Internet of Things Journal*, vol. 9, no. 12, pp. 10327–10339, 2021.
- [11] J. Zhang, J. Zhang, E. Björnson, and B. Ai, "Local partial zero-forcing combining for cell-free massive MIMO systems," *IEEE Trans. on Commun.*, vol. 69, no. 12, pp. 8459–8473, 2021.
- [12] S. Chen, J. Zhang, E. Björnson, J. Zhang, and B. Ai, "Structured massive access for scalable cell-free massive MIMO systems," *IEEE Journal on Selected Areas in Commun.*, vol. 39, no. 4, pp. 1086–1100, 2020.
- [13] L. P. Schulz, C. Schappmann, and G. Bauch, "Scalable cell-free massive mimo with fully distributed large-scale fading decoding," in *Proc, IEEE ISWCS*, Rio de Janeiro, Brazil, July 2024.
- [14] M. S. A. Khan, S. Agnihotri, and R. Karthik, "Comments on "Local partial zero-forcing combining for cell-free massive MIMO systems"," *IEEE Trans. on Commun.*, vol. 73, no. 12, pp. 14986–14989, 2025.
- [15] M. Medard, "The effect upon channel capacity in wireless communications of perfect and imperfect knowledge of the channel," *IEEE Trans. on Inf. theory*, vol. 46, no. 3, pp. 933–946, 2002.
- [16] T. L. Marzetta, E. G. Larsson, H. Yang, and H. Q. Ngo, *Fundamentals of massive MIMO*. Cambridge University Press, 2016.
- [17] E. Björnson, J. Hoydis, and L. Sanguinetti, "Massive MIMO networks: Spectral, energy, and hardware efficiency," *Foundations and Trends® in Signal Processing*, vol. 11, no. 3-4, pp. 154–655, 2017.
- [18] G. Interdonato, M. Karlsson, E. Björnson, and E. G. Larsson, "Local partial zero-forcing precoding for cell-free massive MIMO," *IEEE Trans. on Wireless Commun.*, vol. 19, no. 7, pp. 4758–4774, 2020.
- [19] A. Lozano, A. M. Tulino, and S. Verdú, "Multiple-antenna capacity in the low-power regime," *IEEE Trans. on Inf. Theory*, vol. 49, no. 10, pp. 2527–2544, 2003.
- [20] A. M. Tulino and S. Verdú, "Random matrix theory and wireless communications," *Found, and Trends® in Commun. and Inf. Theory*, vol. 1, no. 1, pp. 1–182, 2004.
- [21] H. Li and Z. Lin, "Accelerated proximal gradient methods for nonconvex programming," *Advances in neural inf. process. systems*, vol. 28, 2015.
- [22] C. Hao, T. T. Vu, H. Q. Ngo, M. N. Dao, X. Dang, C. Wang, and M. Matthaiou, "Joint user association and power control for cell-free massive MIMO," *IEEE Internet of Things Journal*, vol. 11, no. 9, pp. 15823–15841, 2024.
- [23] T. T. Vu, D. T. Ngo, M. N. Dao, S. Durrani, and R. H. Middleton, "Spectral and energy efficiency maximization for content-centric C-RANs with edge caching," *IEEE Trans. on Commun.*, vol. 66, no. 12, pp. 6628–6642, 2018.